

Swiss Soft Days

22nd Edition
Paul Scherrer Institut

Friday, March 2nd 2018



Program
&
Abstracts

Swiss Soft Days 22

2. March 2018, 10:00 – 17:30 Paul Scherrer Institut, Villigen - PSI West, Auditorium

09:45-10:15 Registration and coffee

10:15-10:25 Gasser (PSI)

Welcome

Session I – Colloids / Rheology

10:25-10:45 B. Schroyen (ETH Zürich)

High-frequency rheology on colloidal dispersions: insight into the local structure and interactions

10:45-11:05 G. Colombo (ETH Zürich)

High-speed confocal imaging of sheared colloidal gels

11:05-11:25 N. Senbil (Univ. Fribourg)

Active microrheology in emulsions glass

11:25-11:45 V. Lutz-Bueno (PSI)

Micellar structure and rheology interdependence: SAXS/SANS combined to 1H-NMR measurements

11:45-12:00 Coffee

Session II – Active Soft Matter

12:00-12:20 K. Dietrich (ETH Zürich)

Active Atoms and Interstitials in Two-dimensional Colloidal Crystals

12:20-13:05 A. Fernandez-Nieves (GaTech, Atlanta, USA)

Curvature-induced defect unbinding in active nematic tori

13:05-14:15 Lunch / Poster

Session III – Materials and Methods

14:15-14:35 M.A. Fernandez-Rodriguez (ETH Zürich)

Decoupled 2D Binary Colloidal Alloys for Soft Nanotemplating

14:35-14:55 V. Blair (ETH Zürich)

Transparent Conducting Films of Graphene by Langmuir-Blodgett Deposition: Addressing Aspects of Process Scalability

14:55-15:15 M. Kyropoulou (Univ. Basel)

Light responsive polymer nanocompartments

15:15-15:30 Coffee

15:30-15:50 K. Korzeb (AMI, Univ. Fribourg)

Producing gyroid terpolymer films with long-range order in three dimensions

15:50-16:10 R. Ghanbari (ETH Zürich)

Diffusion of polymers through periodic networks of lipid-based nanochannels

16:10-16:30 F.J. Peaudecerf (ETH Zürich)

Impact of surfactant on the drag reduction potential of superhydrophobic surfaces

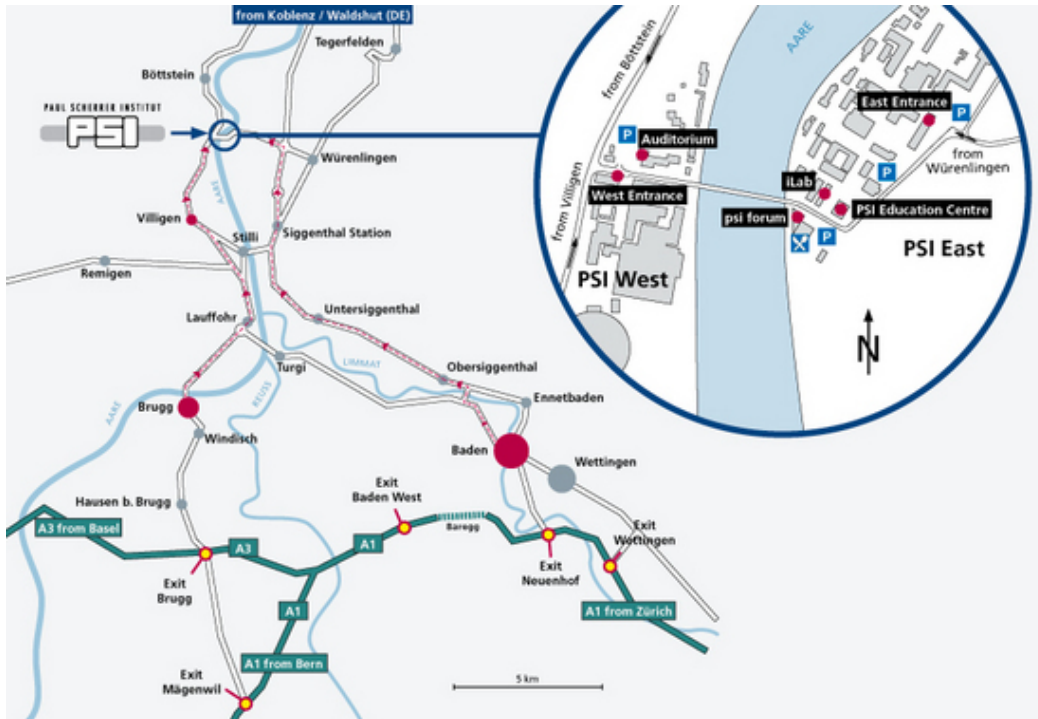
16:30-17:20 Poster Session

17:20-17:30 Gasser (PSI)

Closing Remarks

17:30 Wrap-up with beer, wine and snacks

How to get to the Paul Scherrer Institute



Direction to PSI [Download](#)
Display in route planner [Map24](#)

PSI is located in northern Switzerland, approximately midway between Zürich and Basel. The nearest towns and railway stations are Baden and Brugg. Frequent air and train connections via Zürich or Basel are available from all major European cities.

To find PSI by car

You can reach PSI via Brugg or Baden.

Via Brugg:

Follow the Koblenz–Zürzach signs through Brugg. After passing through Lauffohr and a short hill, branch off to the left towards Remigen/Villigen; then after about 500 m turn right towards Villigen. Approximately 1 km after leaving Villigen you will reach PSI-West. You can drive to PSI-East via the bridge over the river Aare.

Via Baden:

Follow the Koblenz–Zürzach signs through Baden. Drive through Nussbaumen, Untersiggenthal and Station Siggenthal. Approximately 1.5 km beyond the roundabout, follow the sign left towards PSI at the crossroads and you will reach PSI-East. You can drive to PSI-West via the bridge over the river Aare.

Programming of the navigation system:

For PSI West: enter city "Villigen", street "PSI"

It is permitted to use the connecting road across the river Aare.

To reach PSI by public transport

Brugg is on the train line (Zürich–Basel, Zürich–Bern). You can take a public bus (Postauto) from Brugg railway station. Take the Brugg–PSI–Böttstein–Döttingen bus, and within 20 minutes you will arrive at PSI.

How to get to the auditorium

The auditorium is located in the main building of PSI West (WHGA) opposite the bus stop "PSI West". Take the entrance behind the elephant/mammoth shown below.



Abstracts for talks

(In the order of the meeting
schedule)

High frequency rheology on colloidal dispersions: insight into the local structure and interactions

Bram Schroyen^{1,2}, Peter Van Puyvelde², Jan Vermant¹

¹ ETH Zürich, Zürich, Switzerland. ² KU Leuven, Leuven, Belgium

INTRODUCTION: Colloidal dispersions are an interesting class of materials that can display a wide range of rheological behavior such as a yield stress, shear thinning, and shear thickening. Their rheological response is inherently viscoelastic as a result of Brownian relaxation, and is further governed by hydrodynamic and thermodynamic forces. High frequency rheology has proven to be very useful for studying the local microstructure and interactions of colloidal dispersions up to high particle concentrations.

METHODS: In this work, a home-built piezo shear rheometer with optimized alignment and measurement sensitivity is used in parallel with a commercial device to perform frequency sweeps over an extended range from 0.01 – 2000 Hz. This allows investigation of timescales much faster than the diffusional motion of the particles in the dispersion.

RESULTS AND DISCUSSION: The aim of this presentation is twofold. First, the applicability of high frequency rheology as a probe for local dynamics and interactions is illustrated. In order to do so, rheological measurements are performed on sterically stabilized colloidal particles. The softness of the model particles is varied to alter the relative importance of lubrication interactions. The results show that the asymptotic behavior towards the high frequency limit is very sensitive to the dominant interparticle interactions that act on a more local scale. Second, the sensitivity of high frequency rheology to the local dynamics is applied to determine the local microstructure of partially dispersed suspensions. A direct relationship between rheological properties and dispersion state can be derived from the loss modulus in the high frequency hydrodynamic limit. Measurements on partially dispersed spherical silica particles illustrate that in this limit the loss modulus depends only on the hydrodynamic volume occupied by the particles or aggregates, allowing for a direct evaluation of the degree of dispersion.

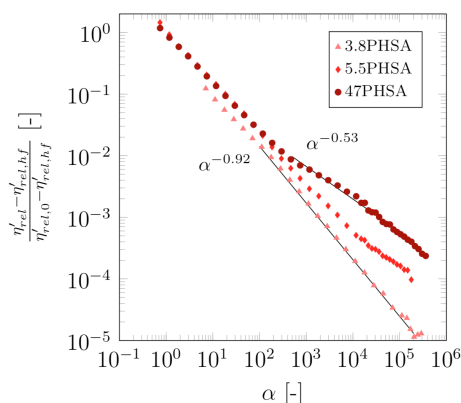


Fig. 1: Linear viscoelastic behaviour (real part of the complex viscosity) of sterically stabilised particles with increasing thickness of the stabilisation layer.

CONCLUSION: Rheology is a robust measurement tool that can offer integrated information over different time and length scales. The results that are presented illustrate the sensitivity of high frequency rheological measurements in particular to the local interactions and microstructure in colloidal dispersions. Description of these local parameters under dynamic conditions play an important role in the understanding of colloidal behavior, which is of interest both for scientific and practical purposes.

REFERENCES: ¹ B. Schroyen, J.W. Swan, P. Van Puyvelde, J. Vermant; **2017**; *Soft Matter*; 13:7897-7906.

ACKNOWLEDGEMENTS: We acknowledge the European Union (EU) Horizon 2020-INFRAIA-2016-1, EUSMI project no. 731019, and the Swiss National Science Foundation, project number 157147

High speed confocal imaging of sheared colloidal gels

Gabriele Colombo and Jan Vermant
ETH Zürich, Zürich, Switzerland.

INTRODUCTION: Colloidal gels represent an interesting family of soft materials. Despite the wide range of possible technological applications, the microstructural details underlying their typical solid-to-liquid transitions upon shear remain poorly understood, therefore posing challenges for industrial formulations. This stems from their hierarchical, strongly heterogeneous structure, lying at the roots of their bulk mechanical properties. The rheology of colloidal gels is very sensitive to the applied flow history and typically shows a complex behavior including a yield stress and thixotropy. Dramatic changes in mechanical properties may well result from subtle, highly localized microstructural changes, which are impossible to resolve using scattering experiments.

METHODS: The experimental approach relies on the quantitative study of the gel microstructure using high-speed confocal microscopy. Microscopic studies under flow are performed using a stress-controlled rheometer with a homemade shear cell for counter-rotation of the lower plate, allowing single particles to be located and tracked for long times at the stagnation plane. The stress is directly measured, so that the link between microscopic observations and nonlinear rheology can be established.

The fast image acquisition (up to 1000 fps in plane) and the enhanced resolution (2x with respect to a normal confocal) of our setup are ideal to study the nonlinear rheology of intermediate to low volume fraction gels, with field of views larger than typically possible.

RESULTS AND DISCUSSION: The shear profile in the measuring gap was validated by particle image velocimetry. It was found to be linear for both plate-plate and cone-plate geometries. Preliminary results were collected on a model depletion colloidal gel, consisting of PHSA grafted PMMA particles, suspended in a density and refractive index matching solvent mixture, to which monodisperse PS was added. Structural rearrangements under shear are readily observed with our setup. At low shear rates, the gel structure coarsens and larger voids are created. At increasingly higher rates, the gel undergoes structural breakdown and eventually flowing aggregates are obtained. The microstructure in this flowing state is anisotropic, with a preferential orientation of microstructural features in the vorticity direction of flow.

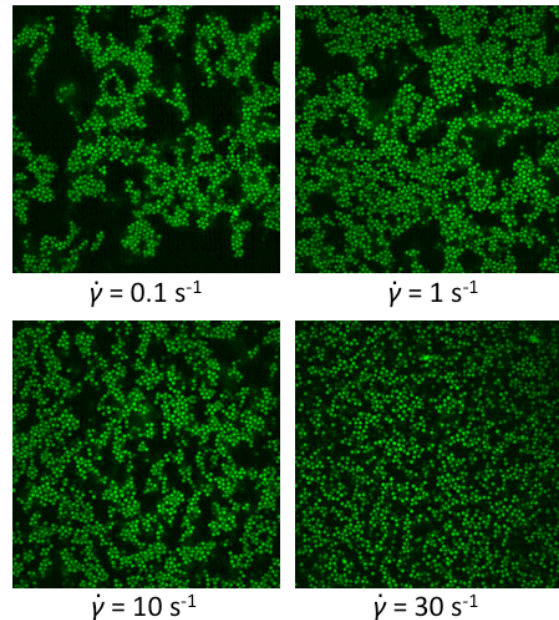


Fig. 1: Snapshots of a model depletion colloidal gel under flow at different shear rates. The particles are $1 \mu\text{m}$ large, while the field of view is $100 \mu\text{m}$ wide

ACKNOWLEDGEMENTS: this work is supported by the Swiss National Science Foundation, project number 157147.

Active microrheology in emulsions glass

N. Şenbil¹, C. Zhang¹, M. Gruber², M. Fuchs², F. Scheffold¹

¹ University of Fribourg, Fribourg, Switzerland. ² Universitat Konstanz, Konstanz, Germany.

INTRODUCTION: Glass has been an inexplicit state of the matter where it exhibits both fluid-like and solid like behaviour. In a colloidal glass system, each particle is bounded with neighbouring ones that form the “cage”. According to the Mode Coupling Theory (MCT), it takes infinite amount of time for the cage to break and release the particle (1). The cage has a strength, which particles cannot overcome, unless an external force is applied. We use active microrheology techniques to overcome the cage strength, in order to determine the threshold force for particle to release. Cage breaking phenomena corresponds to yield stress. Thus, we study the microscopic response of the system and relate to their macroscopic properties.

METHODS: In our experiments, we use oil-in-water shear induced, surfactant stabilized emulsion particles with a diameter of $2\mu\text{m}$ (2). We determine the jamming and glass transition of our system, 64.3% and 58.9% volume fractions respectively, using dynamic light scattering techniques. Polystyrene (PS) beads, which we add in very small number, are identical with the emulsion host particles except their refractive index.

Using time-shared laser trap, we apply constant force on the PS beads and observe their response through light microscope.

RESULTS: Forces varying from 15fN to 132fN applied on the glass sample within 59% to 64% packing fractions. In figure 1a, microscope images of PS bead under 56fN force is shown. If the applied force is high enough, the PS bead moves from one cage to another. However, the response of the system is not always similar under the same conditions if the applied force is around the threshold force. In figure 1b typical trajectories of the probe particle is shown. Each line corresponds to different PS particle under the same force. While in some experiments, PS bead escapes from the cage by making step like motion, there are cases where it cannot break the cage at all, which is a signature of the glass.

Under forces much higher than the critical force, probe melts the sample and the sample acts like a fluid. However, if the force is lower than the critical force, the sample behaves like a solid.

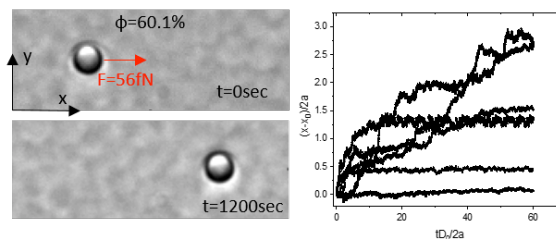


Fig. 1: Trajectory of PS bead embedded in a 60.1% volume fraction sample under 56fN force. a) Position of PS at $t=0$ and 1200seconds later. b) Various trajectories of different PS beads under 56fN force along the direction of the applied force.

DISCUSSION & CONCLUSIONS: Through our experiments, we identify a critical force to yield the system up to around 61%. However, above 61% the force required to release the particle increases dramatically. We compare our results to MCT. Experiments and the MCT agrees well close to glass transition. Moreover, we investigate solid and fluid- like response of the sample at various points within the glass regime under very small and very high forces.

REFERENCES:

1. Gruber M, Abade GC, Puertas AM, Fuchs M. Active microrheology in a colloidal glass. *Physical Review E*. 2016;94(4):19.
2. Zhang C, Gnan N, Mason TG, Zaccarelli E, Scheffold F. Dynamical and structural signatures of the glass transition in emulsions. *J Stat Mech-Theory Exp*. 2016:26.

ACKNOWLEDGEMENTS: We acknowledge support from Swiss National Science Foundation (project number 149867) .

Micellar structure and rheology interdependence: SAXS/SANS combined to $^1\text{H-NMR}$ measurements

V. Lutz-Bueno^{1,2}, M. Liebi^{2,3}, J. Kohlbrecher², P. Fischer¹

¹Institute of food, nutrition and health, ETH Zurich, 8092 Zurich, Switzerland ²Paul Scherrer Institute, 5232 Villigen, Switzerland and ³Current address: Chalmers University of Technology, 4128 Göteborg, Sweden.

INTRODUCTION: We employ small-angle scattering of X-rays SAXS and neutrons SANS to characterize the rheological response of complex fluids. Micellar fluids are used as model systems to investigate self-assembly, micellar growth and viscoelasticity. SAXS and SANS contrast combined to proton-nuclear magnetic resonance $^1\text{H-NMR}$ provide an important link between nanostructure and macroscopic behaviour of self-assembling complex fluids.

METHODS: We focus on the addition of sodium salicylate (NaSal) to hexadecyltrimethylammonium chloride and bromide (CTAC and CTAB), which have distinct counterions, but the same headgroup and hydrophobic tail. The viscoelastic response, relaxation mechanisms and micellar dimensions were measured by rheology, SANS, SAXS and $^1\text{H-NMR}$. The results are based on experiments performed at the Swiss Spallation Neutron Source, SINQ, and Swiss Light Source, cSAXS, at Paul Scherrer Institute [1].

RESULTS AND DISCUSSION: Figure 1 illustrates the anisotropic growth of cationic surfactant aggregates from globular to wormlike micelles upon the addition of salt. The fundamental charged interactions among the surfactant headgroup, tail and counterion depend on the presence of neutralizing additives such as salts. Neutralization can be used to tune molecular self-assembly to specific length scales and control the macroscopic viscoelasticity and structure-flow interdependence.

SANS signals are sensitive to the contrast between the solvent (D_2O) and the hydrocarbonic core of the micelles, while SAXS has a high contrast for the inner structure of the polar shell, because of its high electron density compared to the solvent (water). By measuring the bulk solutions with different radiations, we statically access the most important sample dimensions that correlate to the changes in rheology. Figure 2 illustrates the distinct contrast of CTAC for SANS and SAXS upon NaSal addition and the impact on rheology. The charge density, aggregation number and inter/intra-micellar repulsions were obtained for each sample by fitting a common structure factor to different form factors: dense core for SANS, and core-shell for SAXS. Anisotropic micellar growth

from globular to wormlike micelles, which defines the rheological properties, was tuned by neutralization of intra and inter-micellar interactions. The amount of salt R^* (in Figure 1), when exponential micellar growth starts, depends only on the number of dissociated counterions in the polar shell, which differs in the case of bromide and chloride [2]. The maximum zero-shear viscosity of the solution, $\eta_{0,\text{max}}$, depends on the fluid's formulation. The shape and charge of the surfactant headgroup defines the depth of penetration of additive molecules into the micellar polar shell. This shields the hydrocarbonic core from water and enhances the viscoelastic response.

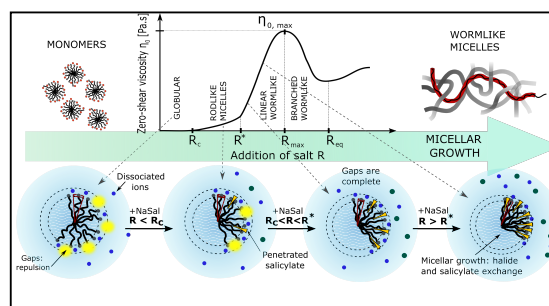


Fig. 1: Structure and micellar cross-section upon salt addition. Adapted from [2].

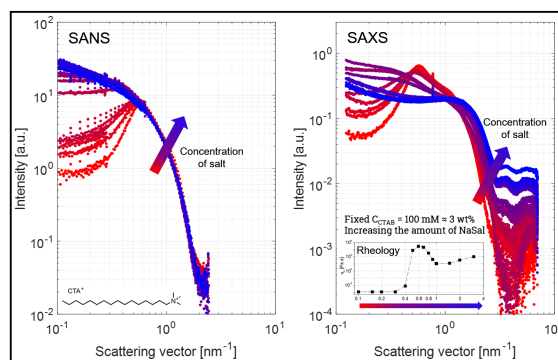


Fig. 2: SANS and SAXS profiles as a function of salt concentration, leading to anisotropic micellar growth. Adapted from [3].

REFERENCES: [1] V. Lutz-Bueno. ETH Zurich, Dissertation Nr. 23650 (2016). [2] V. Lutz-Bueno, M. Liebi, R. Pasquino, J. Kohlbrecher and P. Fischer. *Langmuir*, 32 (17), 4239 (2016). [3] V. Lutz-Bueno, M. Liebi, J. Kohlbrecher and P. Fischer. *Langmuir*, 33 (10), 2617 (2017).

ACKNOWLEDGEMENTS: The Swiss National Foundation is acknowledged for funding (Project No. 22 12-2).

Active Atoms and Interstitials in Two-dimensional Colloidal Crystals

K. Dietrich¹, G. Volpe², M. Sulaiman³, D. Renggli¹, I. Buttinoni^{1,3}, L. Isa¹

¹ ETH Zürich, Zürich, Switzerland. ² University of Gothenburg, Göteborg, Sweden.

³ University of Oxford, Oxford, United Kingdom.

INTRODUCTION: Artificial microswimmers, such as self-propelling colloidal particles, are promising candidates to address transport issues in many nano- and microtechnological applications.¹ Propulsion can be either triggered by external uniform magnetic or electric fields or by an internal conversion of fuel into a driving force, all coupled to a broken symmetry in the particle shape or surface properties.² In spite of the growing interest around these novel man-made active materials, experimental results on self-propelling particles are often limited to systems of swimmers in homogeneous media. However, complex environments, including porous media, fluids under flow and liquid interfaces are ubiquitous in nature. In a previous work we investigated the single particle motion of a specific system of Janus-microswimmers at a water-oil interface and found that these particular particles adsorb in two complementary configurations which affect their propulsion speed and their spatial configuration.³ We now study consecutively, experimentally and numerically, the motion of a self-phoretic active particle in two-dimensional loosely-packed colloidal crystals at liquid interfaces to probe interactions with more complex environments.

METHODS: As model microswimmers, we have used Pt-coated polystyrene particles that undergo active motion due to the catalytic decomposition of H_2O_2 across the Pt-cap.⁴ We spread these particles at a water-oil interface together with passive colloids of the same kind which form two-dimensional loosely-packed lattice structures due to dipolar interactions and incorporate the active swimmers in their two major configurations. Experimental results are compared to Brownian dynamics simulations.

RESULTS: Two scenarios emerge depending on the interaction between the active particle and the lattice: the active particle either navigates throughout the crystal as an interstitial or is part of the lattice and behaves as an active atom, Fig. 1(a-b).

DISCUSSION & CONCLUSIONS: Active interstitials undergo a run-and-tumble-like motion, with the passive colloids of the crystal acting as tumbling sites, Fig. 1(c). Instead, active atoms exhibit an intermittent motion, which stems from the interplay between the periodic potential

landscape of the passive crystal and the particle's self-propulsion, Fig. 1(d). Our results constitute the first step towards the realization of non-close-packed crystalline phases with internal activity.

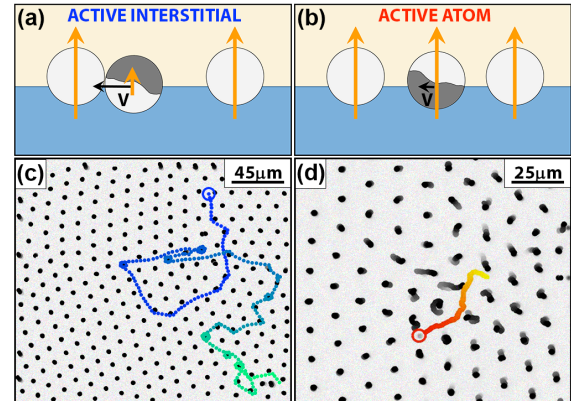


Fig. 1: Active particles in a colloidal crystal. (a,b) Interaction between active and passive particles at the water-oil interface: (a) active interstitial and (b) active atom. The orange arrows sketch the magnitude of the dipolar coupling. (c,d) Experimental trajectories. Blue: active interstitial. Red: active atom. Black: passive colloids. The color gradients represent time from $t = 0$ s (green/yellow/gray) to $t = 30$ s (blue/red/black).

REFERENCES: ¹ S. Sundararajan et al, **2008**, Nano letters, 1271-1276.

² C. Bechinger et al., **2016**, Rev. Mod. Phys., 045006.

³ K. Dietrich et al., **2017**, New J. Phys., 065008.

⁴ J. R. Howse et al., **2007**, PRL, 048102.

ACKNOWLEDGEMENTS: We thank Paolo Margaretti for discussions and Chiao-Peng Hsu for AFM measurements. KD, IB and LI acknowledge financial support from the Swiss National Science Foundation grant PP00P2 144646/1 and the ETH Zurich research grants ETH-16 15-1 and FEL-02 14-1. IB acknowledges support from the European Commission with Marie Skłodowska-Curie individual Fellowship (grant number 747029). GV acknowledges funding by the European Commission with ERC Starting Grant ComplexSwimmers (grant number 677511).

Invited Lecture

Curvature-induced defect unbinding in active nematic tori

[Alberto Fernandez-Nieves](#)

School of Physics, Georgia Institute of Technology, Atlanta, USA.

We will discuss our recent results with active nematics on toroidal surfaces and show how, despite the intrinsic activity and out-of-equilibrium character of our system, we still observe remnants of the expected curvature-induced defect unbinding predicted for nematics in their ground state. In our experiments, however, the number of defects is far larger than what one would expect for conventional nematics. In addition, these defects move throughout the toroidal surface and explore "phase space", bringing about interesting analogies with what we could call the high-temperature limit of a nematic liquid crystal. We unravel the role of activity by comparing our results to numerical simulations, which additionally allows us to perform defect microrheology to obtain the material properties of the active nematic.

Decoupled 2D Binary Colloidal Alloys for Soft Nanotemplating

M.A.Fernandez-Rodriguez¹, M.N.Antonoupoulou¹, L.Isa¹.

¹ETH Zürich, Switzerland.

INTRODUCTION: 2D binary colloidal alloys are useful structures as colloidal models and for nanofabrication applications. Up to now, only close-packed binary colloidal assemblies on a substrate have been reported. We instead report a versatile sequential deposition method using differently sized microgels. We are able to produce complex assemblies with decoupled density gradients for the two particles and with fine control over the interparticle distance. The delicate interplay between capillary attraction and steric repulsion at an oil-water interface allows obtaining a broad range of crystalline microstructures. After deposition on a silicon wafer, such assemblies can be further used as masks for wet etching to obtain Vertically Aligned Nanowires (VA-NWs) with applications in photonics, cell transfection or superhydrophobic surfaces [1].

METHODS: The microgels were synthesized with standard protocols. They are core-shell particles composed of cross-linked N-isopropylacrylamide as the main monomer and methacrylic acid or N-(3-aminopropyl) methacrylamide hydrochloride as co-monomers, for the big and small microgels, respectively. Additionally, microgels without co-monomer were also synthesized.

RESULTS, DISCUSSION & CONCLUSIONS:

A Langmuir trough enabled depositing the microgels from the water/hexane interface onto silicon substrates. In order to get the binary assemblies, sequential depositions of the microgels of different sizes were performed. This protocol allows the independent control of the interparticle distance for each particle type, e.g. achieving a gradient of interparticle distance for the small microgels while the big microgels are kept at a fixed interparticle distance. Moreover, through the fine-tuning on the microgel architecture and of the deposition parameters, square lattices can be obtained thanks to a fine balance between capillary quadrupolar attraction and steric repulsion at the water/hexane interface. AFM images were taken to characterize the transferred assemblies (see Fig. 1a). HF wet etching enabled producing VA-NWs using the binary colloidal assembly as masks for metal-assisted chemical etching (see Fig. 1b). Such VA-NWs have interesting optical properties, ranging from iridescence to structured colors and

wavelength modulation, depending on the geometry of the VA-NWs, which we characterized with reflectivity measurements and compared to simulations.

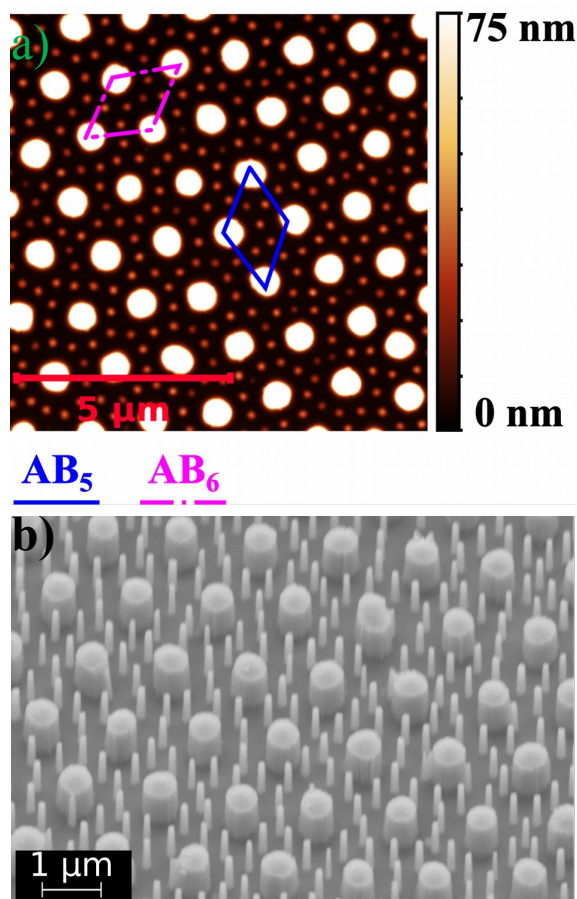


Fig. 1: a) AFM image of microgels on a silicon wafer forming 2D binary colloidal alloys with AB₅ and AB₆ unit cells. b) VA-NWs obtained using the microgels as masks in wet-etching.

REFERENCES: ¹M.Rey, R.Elnathan, R.Ditcovski, K.Geisel, M.Zanini, M.A.Fernandez-Rodriguez, V.V.Naik, A.Frutiger, W.Richtering, T.Ellenbogen, N.H.Voelcker, and L.Isa; **2016**; *Nano Letters*, 16:157-163.

ACKNOWLEDGEMENTS: L.I. and M.A.F.R. thanks the SNSF (Grants PP00P2 144646/1 and PP00P2_172913/1) and Swiss SERI (Excellence Postdoc Scholarship 2016.0246).

Transparent Conducting Films of Graphene by Langmuir-Blodgett Deposition: Addressing Aspects of Process Scalability

V. Blair, J. Vermant

Soft Materials, Department of Materials, ETH Zürich, Zürich, Switzerland.

INTRODUCTION: Despite the ever-growing interest in graphene as a feasible alternative to ITO for conductive film applications, the processing of such materials in a low cost and environmentally gentle manner can still be drastically improved from current vapour deposition processes. Production of graphene by exfoliation and stabilisation in the liquid-phase avoids the generation of toxic waste gases produced during current vapour deposition processes and facilitates straightforward introduction of the material to liquid interfaces. Here we employ such exfoliation methods in the production of graphene flakes, which are then introduced to the water-air interface and subsequently transferred to solid substrates for the production of electrically conductive films. In-line characterisation is integrated into the interfacial transfer process through in-situ measurement of electrical conductivity and alternative methods of material transport are explored to address scalability restraints of the traditional Langmuir-Blodgett deposition technique.

METHODS: Graphene is produced from graphite foil by a modified protocol from that described in Parvez et. al¹. The resulting graphene dispersion in N-Methyl-2-Pyrrolidone (NMP) is diluted with chloroform to allow spreading of the graphene sheets at the water-air interface. Surface pressure – Area curves are recorded in a Langmuir trough with platinum Wilhelmy plate to record changes in surface tension. Compression of the material is achieved by either mechanical compression or generation of Marangoni stresses over the surface, achieved through exposure of the liquid surface to vapour of IPA or by small temperature differences applied over the interface. Electrical conductivity of the interface is measured throughout the transport process until electrical percolation of the sheets is achieved, at which point the interfacial material is transferred to silica or glass substrates for further characterisation.

RESULTS: The liquid-exfoliated graphene sheets produced via this method (typical appearance shown in *Figure 1a*) are typically several hundred nanometres to one micron in diameter and produce mechanically percolated solid-like networks when compressed (*Figure 1b*). The onset of mechanical percolation of the sheets is paralleled by the

emergence of electrical conductivity (*Figure 1c*), which can be simultaneously monitored during the compression process. Films of graphene sheets typically between 1-2 nm in thickness can be deposited (*Figure 1d*) to make electrically conductive films of typically 5-10 S/cm.

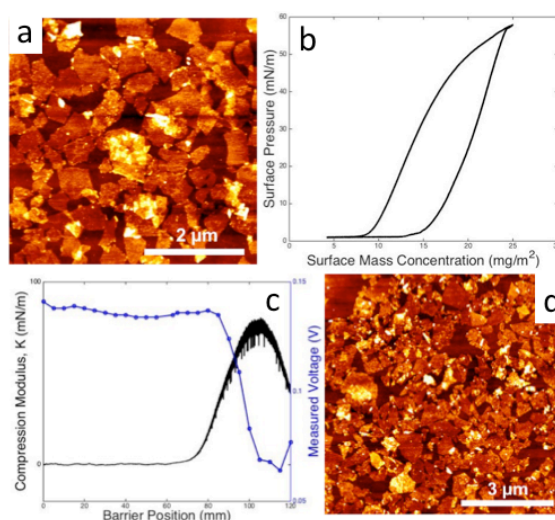


Fig. 1: (a) AFM image of exfoliated graphene sheets. (b) Surface pressure-Area curve of graphene at water-air interface. (c) Effect of compression state on electrical resistivity of interface. (d) Graphene monolayer deposited using the vapour of IPA.

DISCUSSION & CONCLUSIONS: Stable monolayers of graphene can be made directly from untreated graphite when assembled on liquid interfaces. Conductive thin films can be deposited using Langmuir-Blodgett-style techniques where small Marangoni stresses generated at the interface are shown to be as effective as the classical method of mechanical compression. This work highlights the potential for the inherently lab-scale current wet-processing methods to gain a greater level of scalability towards the development of continuous processes.

REFERENCES: ¹ Parvez, Khaled, et al. *Journal of the American Chemical Society* 136.16 (2014): 6083-6091.

ACKNOWLEDGEMENTS: Funding is gratefully acknowledged as part of the Marie Curie ITN, SOMATAI.

Light responsive polymer nanocompartments

M. Kyropoulou, A.Lanzilotto C. E. Housecroft*, E. C. Constable*, W.Meier*, C. Palivan*

Department Physical and Inorganic Chemistry, University of Basel, Mattenstrasse 24a, CH-4002 Basel, Switzerland

INTRODUCTION: Use of stimulus-sensitive nanostructures is promising for therapeutic and diagnostic approaches by producing responses to the presence of specific molecules or conditions either by changing properties or by acting “on demand”¹. Here we introduce an optimized light-sensitive nanoreactor based on encapsulation of a water soluble alkylpyridinio-porphyrin photosensitizer inside polymer vesicles. Amphiphilic block copolymer, poly(2-methyloxazoline)-blockpoly(dimethylsiloxane)-block-poly(2-methyloxazoline), was used to encapsulate porphyrin inside the cavity of vesicles.

METHODS: Polymer nanocarriers were optimized in terms of size, stability and generation of singlet oxygen 1O_2 based on a combination of light scattering, TEM, ESP and emission spectroscopy. Regarding 1O_2 generation, vesicles have been tested by oxidizing the aminoacid methionine in a solution of D_2O . Methionine was irradiated in D_2O by means of a LED ($\lambda_{max} = 660$ nm) for 24 hours in the presence of the polymer vesicles.

A step further, is an in vitro study of the system by bioluminescence of bacteria E.Coli and then the biological evaluation of the polymer vesicles as candidates for photodynamic therapy has been assessed.).

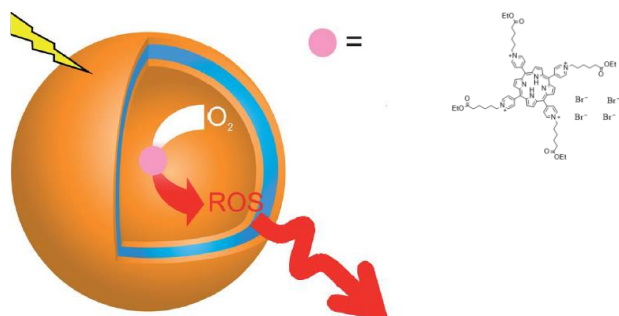


Fig. 1: Schematic representation of a porphyrin loaded polymersome Table 1. Relative allocation and amount of resources in research.

RESULTS AND DISCUSSION:

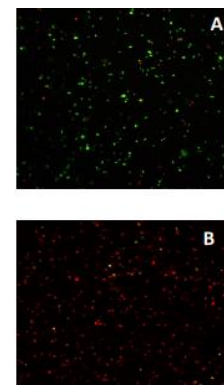
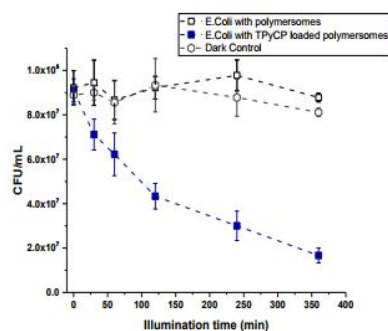


Fig. 2: CFU E. coli monitoring treated with polymersomes 200 μ M of TPyCP after 30, 120, 240 and 360 (blue squares) min of irradiation with LED red light ($\lambda_{exc} = 660$ nm), kept in dark (grey hexagons) with empty polymersomes (black empty squares) in three independent experiments, whereas the confocal laser microscope pictures, bacteria are stained with SYTO 9 (alive, green) and propidium iodide (dead, red) after 0min(A) and 360min(B) illumination time with red LED light ($\lambda_{exc} = 660$ nm)

CONCLUSIONS AND CHALLENGES AHEAD:

- ✓ Successful insertion of a new water soluble porphyrin into polymersomes
- ✓ Release of singlet oxygen
- ✓ In vitro studies: antimicrobial activity (E. Coli culture)
 - ❖ Optimization of the reaction conditions
 - ❖ Exploring possible in vitro cytotoxicity tests

REFERENCES: Patric Baumann, Mariana Spulber, Ionel Adrian Dinu, and Cornelia G. Palivan J. Phys. Chem. B 2014, 118, 9361–9370.

ACKNOWLEDGEMENTS:

Swiss National Science Foundation and NCCR Molecular Systems Engineering for the funding Samuel Lörcher (polymer synthesis)

Producing gyroid terpolymer films with long-range order in three dimensions

K.Korzeb¹, J.A.Dolan^{1,2}, C.Kilchoer¹, N.Abdollahi¹, B.D.Wilts¹, U.Wiesner³, U.Steiner¹, I.Gunkel¹

¹ Adolphe Merkle Institute, Switzerland. ² Institute for Molecular Engineering, University of Chicago, Chicago, IL, United States. ³ Department of Materials Science and Engineering, Cornell University, Ithaca, NY, United States.

INTRODUCTION: The ability of block copolymers (BCPs) to self-assemble into morphologies on the order of 10-100 nm makes them interesting candidates for the use as templates in the fabrication of lithography masks and optical metamaterials[1]. A morphology that is particularly interesting for optical metamaterial applications is the gyroid – a bicontinuous and triply periodic cubic morphology. So far, the bottleneck in the polymer-templated fabrication of gyroid metamaterials has been the generation of gyroid polymer films with long-range order (grains in the order from 10 to 100 μm). Here we show that long-range order in gyroid BCP films can be achieved in three dimensions through a combination of solvent vapour annealing (SVA) and a subsequent slow controlled drying of the polymer films.

METHODS: Thin films of a polyisoprene-*b*-polystyrene-*b*-poly(glycidyl methacrylate) (ISG) triblock terpolymer ($M_n = 67.4$ kg/mol) were fabricated by spin coating. *In situ* grazing incidence small-angle x-ray scattering (GISAXS) was employed to identify the order-disorder transition in ISG terpolymer films during SVA in tetrahydrofuran. After SVA, dried polymer thin films were examined by atomic force microscopy (AFM) and GISAXS. Gyroid polymer films were used as template for the fabrication of gold gyroids on conductive fluorine-doped tin oxide (FTO) coated glass by means of electrodeposition. The gold gyroid replica were characterized using scanning electron microscopy, small-angle X-ray scattering and optical microscopy.

RESULTS: *Figure 1a* shows an AFM phase image of a THF-annealed ISG terpolymer film, which has been slowly dried over the course of 44 hours. A well-ordered hexagonal pattern can be observed that is consistent with the top view of an alternating gyroid with the (111) surface oriented parallel to the substrate as shown in *Figure 1b*. The gyroid morphology has been confirmed by GISAXS analysis (*Figure 1c*). The gold replica of ISG gyroid films exhibits a well-ordered structure throughout the entire thickness of the film as can be seen the cross-sectional SEM image of the replica shown in *Figure 1d*. The gold gyroid exhibits long-range order morphology with grains

having a diameter of about 11-16 μm as determined from polarized optical micrographs (not shown).

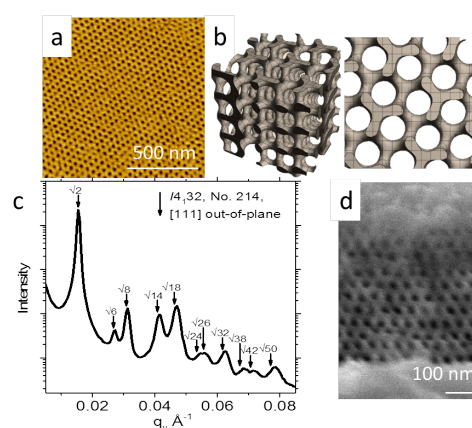


Fig. 1: (a) AFM phase image and (c) 1D GISAXS pattern of an annealed ISG terpolymer film. (b) 3D visualization (left) with (111) surface (right) of the gyroid morphology formed in ISG films. (d) Cross-sectional SEM image of gold gyroid fabricated from the ISG template shown in (a).

DISCUSSION & CONCLUSIONS: Gyroid structures with grains of about 11-16 μm in size were generated by means of controlled solvent vapour annealing of ISG triblock terpolymer film. Gyroids with long-range order were produced by slowly removing the solvent from swollen ISG films in the ordered state. This study provides detailed structural information, which is key to generating well-ordered gyroid terpolymer films that can serve as templates for the fabrication of optical metamaterials

REFERENCES: [1] J.A. Dolan *et al.*; **2014**; *Adv. Opt. Mat.*; 3:12-32.

ACKNOWLEDGEMENTS: This research was supported by the SNSF through grant number 163220, the Adolphe Merkle Foundation, and the EU's Horizon 2020 research & innovation programme under the Marie Skłodowska-Curie grant agreement No 706329/cOMPoSe. The authors also thank the Swiss Light Source, Diamond Light Source, and Advanced Photon Source for beamline access.

Diffusion of polymers through periodic networks of lipid-based nanochannels

R.Ghanbari¹,Salvatore Assenza¹, Abhijit Saha^{1,*}, Raffele Mezzenga^{1,2}

¹ETH Zurich, Food and Soft Materials Science, Department of Health Science & Technology, Institute of Food, Nutrition & Health, Schmelzbergstrasse 9, CH-8092 Zurich, Switzerland

²ETH Zurich, Department of Materials, Wolfgang-Pauli-Strasse 10, 8093 Zurich, Switzerland

*Present address: Department of Chemistry, University of Washington, Seattle, WA, USA, 98195

INTRODUCTION: We present an experimental investigation on the diffusion of unfolded polymers in the triply-periodic water-channel network of inverse bicontinuous cubic phases(BCP). IBCPs are an intriguing class of lipid-based membranes characterized by a three-dimensional periodic structure at the nanometer scale. The periodic and geometrical features of IBCPs make them ideal biomimetic systems for several nanotechnological applications. Depending on the chain size, our results indicate the presence of two different dynamical regimes corresponding to Zimm and Rouse diffusion [1]. We support our findings by scaling arguments based on a combination of blob and effective-medium theories, and suggest the presence of a third regime where dynamics is driven by reptation.

METHODS: In the Release setup, the cubic phase is formed by mixing the monolinolein with a dilute solution of monodispersed PEG in water. The IBCP is then inserted into a cylindrical tube and put in contact with a receiving chamber filled with Milli-Q water. In the Diffusion setup, the IBCP is initially free of polymers. When inserted into the tube, it is placed between a delivering chamber containing the PEG solution and a receiving one filled with Milli-Q water.

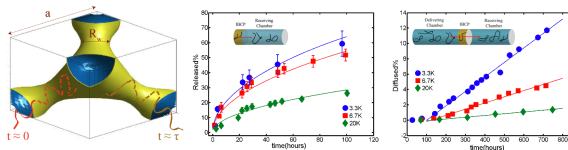


Fig. 1: Left panel: Four-fold repeating structure and representative diffusing polymer. Central Panel: Examples of Release profiles. Inset: sketch of the Release setup. Right panel: Diffusion profiles. Inset: schematics of the Diffusion setup.

Small-angle X-ray scattering (SAXS) measurements were used to determine the symmetry and lattice parameters of the IBCP.

RESULTS: We performed a series of Release experiments, each involving solution of PEG with a given molecular weight. The dependence of the total fraction of released molecules Q on time reads

$$Q(t) = 1 - \frac{8}{\pi^2} \sum_{n=0}^{\infty} \frac{1}{(2n+1)^2} e^{-\frac{(2n+1)^2 \pi^2 D_m t}{4h^2}} \quad (1)$$

Results acquired by Release setup are further supported by experiments performed with the Diffusion setup. Larger polymers diffuse more slowly in both cases. One can notice that Diffusion kinetics is slower than its Release counterpart.

DISCUSSION & CONCLUSIONS:

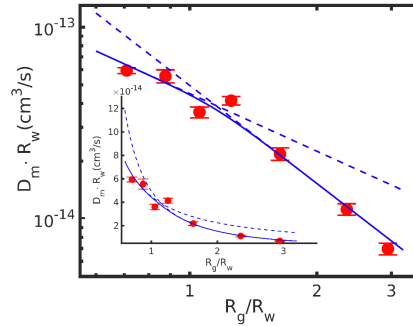


Fig. 2: Rescaled diffusion coefficient $D_m R_w$ as a function of the ratio R_g/R_w for the same set of data considered in Figure 3 in log-log (main plot) and lin-lin (inset) scales.

A customary approach to provide a single fit consists in considering a double power law of the form

$$D_m R_w \sim \left(\frac{1}{c} \frac{R_g}{R_w}\right)^{-1} \left[1 + \left(\frac{1}{c} \frac{R_g}{R_w}\right)^{\frac{1}{\alpha}} \right]^{\alpha \left(-\frac{1}{v} + 1\right)} \quad (9)$$

We have here performed for the first time a systematic study on the diffusion properties of unstructured polymers in inverse bicontinuous cubic phases. Combining considerations from effective medium theories and scaling arguments, we elucidated how the interplay between length scales determines the transport properties of unfolded macromolecules within cubic phases, thus providing a basis to devise optimized systems for their practical applications [2].

REFERENCES:

¹M. Doi et al; The theory of polymer dynamics; 1988; 73

²R. Ghanbari et al; 2017; *Langmuir*; 33:3491-3498.

ACKNOWLEDGEMENTS: The authors are indebted to N.Hermann and E. Heer.

IMPACT OF SURFACTANT ON THE DRAG REDUCTION POTENTIAL OF SUPERHYDROPHOBIC SURFACES

F.J.Peaudecerf¹, J.R.Landel², F.Temprano-Coletto³, F.Gibou³, R.E.Goldstein⁴, P.Luzzatto-Fegiz³

¹ ETH Zürich, Zürich, Switzerland. ² University of Manchester, Manchester, UK.

³ University of California, Santa Barbara, USA. ⁴ University of Cambridge, Cambridge, UK.

INTRODUCTION: Superhydrophobic surfaces (SHSs) have the potential to achieve large drag reduction for internal and external flow applications. However, experiments have shown inconsistent results, with many studies reporting significantly reduced performance. Recently, it has been proposed that surfactants could be responsible for this reduced performance, by creating adverse Marangoni stresses under flow conditions [1] (Fig. 1). Yet, testing the role of surfactants on SHSs is challenging. Careful experiments with purified water already show large interfacial stresses and, paradoxically, adding surfactants yields barely measurable drag increases [2].

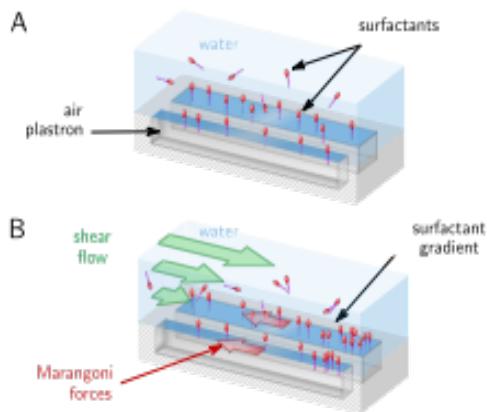


Fig. 1: (A) Surfactants present in water adsorb at the air–water interface of the plastron of SHSs. (B) In the presence of an external flow, surfactants distribute in gradients between stagnation points. The resulting Marangoni forces resist the flow.

METHODS AND RESULTS: To test the surfactant hypothesis, we perform the first numerical simulations of flows over a SHS inclusive of surfactant kinetics [3]. These simulations reveal that surfactant-induced stresses are significant at extremely low concentrations, potentially preventing any slip at the air–water interface (the “plastron”) even in nominally clean conditions.

To provide an experimental metric of surfactant effects, we perform microchannel experiments with thermally-controlled SHSs consisting of

streamwise parallel gratings [3] as sketched on Fig. 1. Under a steady pressure gradient generating a flow in the channel, we observe an immobilized interface at the plastron and the absence of free-slip. After a loading phase with steady flow, we drop the driving pressure gradient to zero. We observe a backflow developing at the plastron, which can only be explained by surfactant gradients formed during the loading phase.

These effects, which arise from the interplay of trace surfactant and flow, are highly sensitive to geometry. We exploit this fact in [4] to show that similar surfactant effects can display maze-solving abilities, as shown in Fig. 2.

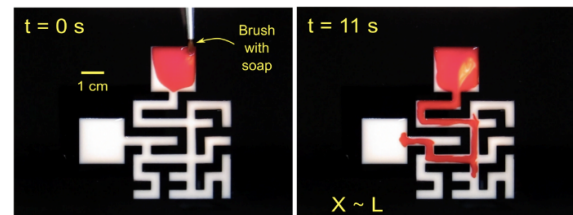


Fig. 2: Interaction between endogenous and exogenous surfactant can generate a fluid flow solving a maze (from [4]).

DISCUSSION & CONCLUSIONS: This work demonstrates the significance of surfactants in deteriorating drag reduction, and thus the importance of including surfactant stresses in SHS models. Our load-and-relax experimental protocol can assess the impact of surfactants in SHS testing and guide future mitigating designs.

REFERENCES: ¹ T.J. Kim; 2012; *Phys.Fluids*; 24:112003. ² D. Schäffel, K. Koynov, D. Vollmer, H.J. Butt, C. Schönecker; 2016; *Phys. Rev. Lett.*; 116:134501. ³ F.J. Peaudecerf, J.R. Landel, R.E. Goldstein, P. Luzzatto-Fegiz; 2017; *PNAS*; 28:7254-7259. ⁴ F. Temprano-Coletto, F. Peaudecerf, J. Landel, F. Gibou, P. Luzzatto-Fegiz; 2017; *Gallery of Fluids Motion*; DOI: 10.1103/APS.DFD.2017.GFM.V0098

ACKNOWLEDGEMENTS: We acknowledge support from the Sackler Foundation, EPSRC, ERC Grant 247333, Mines ParisTech, the Schlumberger Chair Fund, the UCSB Senate and CNSI Challenge Grant, as well as from Churchill and Magdalene Colleges, Cambridge.

Abstracts for posters

(First authors in alphabetic
order)

Confinement-Induced Liquid Crystalline Transitions in Amyloid Fibril Cholesteric Tactoids

Mario Arcari¹, Gustav Nyström¹ and Raffaele Mezzenga¹

¹ *ETH Zurich Department of Health Science and Technology, Schmelzbergstrasse 9, LFO E23 Zurich 8092, Switzerland.*

INTRODUCTION: Understanding and controlling chirality is an important research challenge with broad implications. Unlike other chiral colloids, e.g. nanocellulose or filamentous viruses, amyloid fibrils form nematic phases but appear to miss their twisted form, the cholesteric or chiral nematic phases, despite a well-defined chirality at the single fibril level. Here we report the discovery of cholesteric phases in amyloids, using β -lactoglobulin fibrils shortened by shear stresses. The physical behavior of these new cholesteric materials exhibits unprecedented structural complexity, with confinement-driven ordering transitions between at least three types of nematic and cholesteric tactoids. We use energy functional theory to rationalize these results and observe a chirality inversion from the left-handed amyloids to the right-handed cholesteric droplets. These findings deepen our understanding of cholesteric phases advancing their use in soft nanotechnology, nanomaterials templating and self-assembly.

METHODS: Short and purified amyloid fibrils were achieved through high shear force mechanical cutting followed by dialysis. The settings applied here resulted in a sample average length of ~ 400 nm (determined by statistical analysis of TEM images). The fibril solution was then up-concentrated through reverse osmosis against a 10 wt% PEG solution to achieve an end concentration of 1.3 wt%.

RESULTS & DISCUSSION: Aqueous amyloid fibril dispersions display an isotropic nematic phase transition with a rich phase behaviour of the nematic phase. By nucleation and growth, first homogeneous nematic tactoids emerge that further transform to tactoids with a bipolar director field and later develop to uniaxial cholesteric droplets.

These phase transitions can be explained using a scaling form of the Frank-Oseen elasticity theory. The theoretical model was verified with data from cross-polarized optical light microscope observed in the isotropic-nematic coexistence zone of the amyloid fibril dispersion.

As predicted by the theoretical model, first a threshold for the transition from tactoids with homogeneous to bipolar director fields could be experimentally confirmed (see Fig. 1). Secondly,

the critical size, where the tactoids start to develop a cholesteric twist, was observed.

To determine the handedness of the cholesteric phase, an experimental setup was designed where the right-handedness of the amyloid system could be directly observed. Keeping the left-handedness of the single amyloid fibril in mind, an inversion of the chirality from single particle to cholesteric liquid crystalline phase is observed.

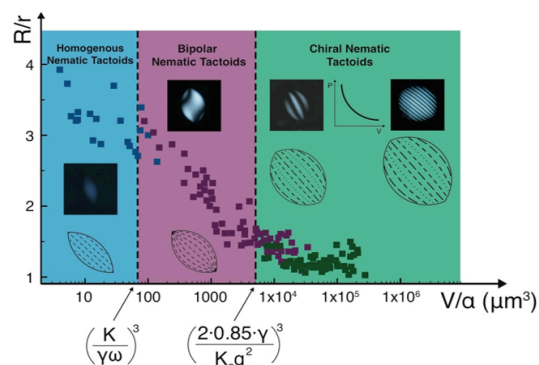


Fig. 1: Nematic-cholesteric phase diagram. The two theoretically predicted threshold volumes for the transition between homogenous (blue area) to bipolar nematic tactoids (purple area) and the transition between bipolar nematic and cholesteric tactoids (green area) are highlighted. Data points for the tactoid aspect ratio versus volume are plotted as blue, purple and green squares for the homogeneous, bipolar and chiral nematic tactoids respectively.

CONCLUSIONS: We have discovered the presence of cholesteric phases in amyloid fibril suspensions, revealing a very rich phase diagram in which size-confinement controls order-order transitions among homogeneous nematic, bipolar nematic and chiral nematic tactoids and we relied on energy functional considerations to rationalize the main experimental findings. We have further shown an inversion of chirality from the left-handed amyloids to the right-handed cholesteric of this new class of chiral biological nanomaterial that provides the basis for understanding its liquid crystalline transitions.

REFERENCES: Confinement-Induced Liquid Crystalline Transitions in Amyloid Fibril Cholesteric Tactoids. *arXiv* **2017**, 1704.04936 & *Nat. Nanotechn.* **2018** - Accepted.

GENERATION OF TOROIDAL SEEDS FOR HETEROGENEOUS NUCLEATION STUDIES OF COLLOIDS

D. Blatman^{1,2}, Y. Chang^{2,3}, A. Fragkopoulos², P. Ellis², U. Gasser¹, A. Fernandez-Nieves²

¹ *Laboratory for Neutron Scattering and Imaging, Paul Scherrer Institut, Villigen, Switzerland.*

² *Soft Condensed Matter Laboratory, Georgia Institute of Technology, Atlanta, USA.*

³ *Texas Tech University, Department of Chemical Engineering, Lubbock USA*

INTRODUCTION: Toroidal seeds are ideal to investigate the effect of heterogeneous nucleation and crystal growth of colloidal systems on curved surfaces. The torus, being positively curved on its outside and negatively curved on its inside, has a rich geometry and is therefore an interesting object to study heterogeneous nucleation.

METHODS: Due to surface tension toroidal droplets will either break [1],[2] into single droplets via the Rayleigh Plateau instabilities and/or shrink [2] to a sphere unless there is an opposing force that stabilizes them. This can be done in a yield stress material [3].

Tori are made through the injection of a fluid into another immiscible material, while the two materials are in relative rotational motion. The process of making a torus can be seen as a 3D printing process, where a needle's tip is printing into a suitable media. The outer continuous phase is chosen to be a yield stress material in order to stabilize the produced tori against the instabilities due to surface tension. Tori can be made in water and oil based yield stress materials. Tori out of a prepolymer solution containing NIPAM monomers (N-Isopropylacrylamide) can be polymerized to produce stable toroidal hydrogels. These can be used as seeds for heterogeneous nucleation experiments when placed into colloidal suspensions. The ratio between the tube diameter of the tori and the diameter of the colloids is expected to determine whether curvature effects will play a significant role on heterogeneous nucleation or not. This is why it is important to minimize the tube diameters of the toroidal hydrogels and bring them close to the colloidal length scale.

RESULTS: Stable toroidal hydrogels of various sizes (from millimeters down to below 100 micrometers in tube diameter) can be made using a 3D printer setup using an automatized stage and be used for heterogeneous nucleation studies using confocal microscopy. It is seen that pNIPAM tori are good to work with pNIPAM colloids, because they do not stick to the surface, thereby minimizing the effect of other interactions on heterogeneous nucleation. On the other hand

PMMA particles do stick to the surface of the tori to some extent. The system of PMMA particles in the organic solvent mixture of Decalin and Cycloheptyl-Bromide is still useful, because it has the advantage that in this environment, the toroidal hydrogels will shrink with respect to their original size in water.

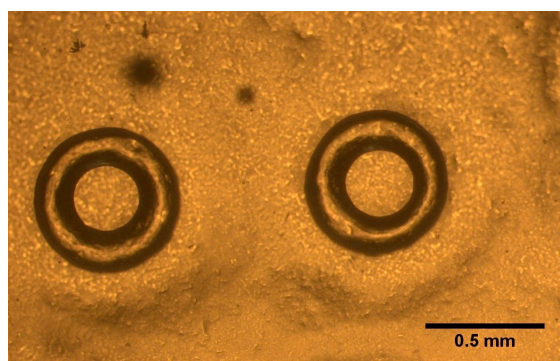


Figure 1 Toroidal droplets in silicone elastomer blend

DISCUSSION & CONCLUSIONS:

By using a yield stress material toroidal droplets can be stabilized against the hydrodynamic instabilities which arise due to surface tension. By using a polymerization process toroidal droplets can be transformed into toroidal hydrogels which can be used as seeds for studying heterogeneous nucleation of colloidal systems.

REFERENCES:

- [1] A A Fragkopoulos, P W Ellis and A Fernandez-Nieves, Teaching Rayleigh–Plateau instabilities in the laboratory, *Eur. J. Phys.* 36 (2015) 055023 (10pp)
- [2] E. Páram, H. Le, and A. Fernandez-Nieves, Generation and Stability of Toroidal Droplets in a Viscous Liquid, *PRL* 102, 234501 (2009)
- [3] E. Páram, H. Le, and A. Fernandez-Nieves : Stability of Toroidal droplets inside yield stress materials, *PHYSICAL REVIEW E* 90, 021002(R) (2014)

Reactive hexayne surfactant for the formation of 2D carbon nanosheets at the liquid-liquid interface

E. Bomal¹, B. Schulte¹, H. Frauenrath¹

¹ *Laboratory of Macromolecular and Organic Materials (LMOM), Institute of Materials, Ecole Polytechnique Fédérale de Lausanne (EPFL), Switzerland*

INTRODUCTION: The liquid-liquid interface is a high energy interface that can be stabilized using interfacially active molecules. The employed surfactants self-assemble at the oil-water interface, exposing their polar head group to water and apolar tail group to the oil phase, allowing the use of the liquid-liquid interface as template for two-dimensional assembly. Here, we report the in-situ formation of 2D carbon nanosheets at the liquid-liquid interface, starting from reactive hexayne surfactants that undergo two-dimensional interfacial polymerization under mild conditions.

Our laboratory had previously used a reactive, carbon-rich surfactant to fabricate carbon nanosheets at the air-water interface at room temperature [1]. In the work presented here, we employ an amphiphile comprising a phosphonic acid head group, as well as a hexayne segment, which is made up of 12 sp-hybridized carbon atoms and is reactive towards a rearrangement into carbon allotropes.

METHODS: The liquid-liquid interfaces studied are the toluene/water and chloroform/water interfaces. The pH of water was adjusted using 1M NaOH and 1M HCl solutions. The transition from molecular surfactant stabilization to a colloidal stabilization of the interface can be followed by drop tensiometry. The crosslinking can further be induced using UV irradiation. Scanning electron microscopy was performed on the Langmuir-Blodgett transferred carbon nanosheet. The chemical structure of the formed nanosheets are investigated in depth through UV-Vis, Raman and IR spectroscopy.

RESULTS: The drop tensiometry images show the formation of a buckled interface upon change of interfacial area, which suggest the formation of a carbon nanosheet at the liquid-liquid interface (Figure 1). This nanosheet is formed spontaneously between pH 4 and pH 8, whereas for lower pH values a UV irradiation step seems to be necessary to produce a film. The formation of a continuous carbon film was confirmed by electron microscopy.

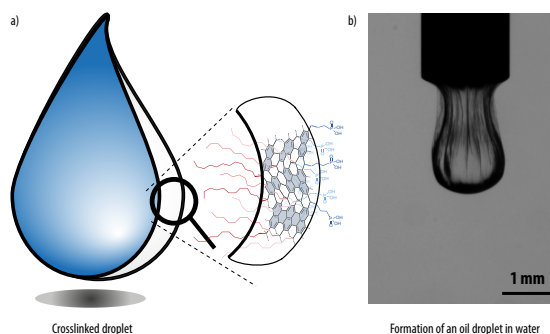


Figure 1: a) Carbonization at the liquid-liquid interface upon mild heat or UV treatment b) buckling of the chloroform/water interface due the formation a carbon nanosheet at the interface

DISCUSSION & CONCLUSIONS: This precursor amphiphiles therefore self-assemble at the oil-water interface and spontaneously react to first form a cross-linked organic membrane. This membrane can be further cross-linked by mild heat treatment or UV irradiation, resulting in a molecularly thin two-dimensional carbon nanosheet with a “Janus-type” functionalization, that is, one face decorated with the polar head groups and the other one with apolar alkyl tails. In contrast to the molecular precursor surfactants, the nanosheets present distinctive properties of a Pickering emulsion, such as buckling upon a change in the interfacial area.

REFERENCES: [1] Schrettl, S.; Frauenrath, H. et al, *Nature Chem.* **2014**, *6*, 468.

Solution and gel-properties of ultra-high molecular weight polyethylene in good and poor solvents

A.Brem, J.Vermant, T.A.Tervoort

ETH Zürich, Zürich, Switzerland

INTRODUCTION: Recently the gel-spinning of high-performance polyethylene (HPPE) fiber precursor from “green” solvents, such as vegetable oils, was demonstrated [1]. In comparison to the use of precursor fibers crystallized from traditional solvents, such as decalin, for a given polymer concentration, even better properties could be achieved by using precursor fibers crystallized from solvents with a remarkably poorer solvent quality.

The reasons for the improved performance were not evident and the results are questioning the established concept of the reduced entanglement density in solution being solely responsible for drawability. In this study, a systematic approach, aiming at the identification of factors affecting drawability in the gel-spinning process as a function of solvent quality, is presented. The study is divided into four parts, corresponding to four main stages of the gel-spinning process: rheological properties of the polymer solution, the gelation process, mechanical properties of the resulting gel and drawing behavior of the polymer fiber precursor. Throughout the study, measurements were performed for different polymer concentrations in good and poor solvents

METHODS: First, the linear viscoelastic behavior of polymer solutions is investigated, with a focus on differences in the molecular weight between entanglements and the zero-shear viscosity of solutions of good and poor solvents (at equal volume fraction). Second, the gelation process is analyzed using the Winter-Chambon method for near critical gels, addressing gelation time, gel strength S and relaxation exponent n in dependence of undercooling (see Equation 1). The final gel and fiber precursor are characterized by the means of isothermal dynamic mechanical analysis in shear and compression, as well as simple uniaxial compression. Finally, the correlation of the observed properties of the gel, with the drawability of the polymer fiber precursor, will be discussed.

RESULTS: The method of Winter and Chambon was successfully applied to different polyethylene-solvent systems (see Figure 1). The relaxation exponent n is around 0.15 and does not change with solvent quality, neither does the relaxation strength with a value about 2 kPa.

$$G(t) = St^{-n} \quad (1)$$

The gel time is longer for solutions in good solvents at equal undercooling.

In the linear viscoelastic regime in shear, concentrated solutions did not show a change in behaviour on solvent quality.

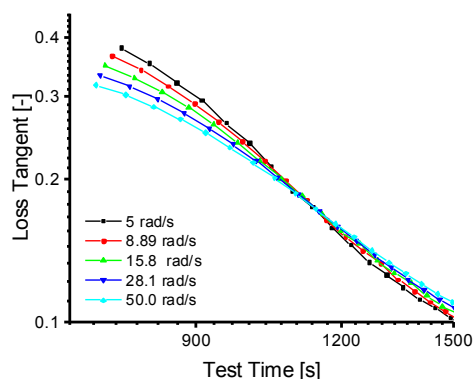


Fig. 1: Course of loss tangent at different frequencies over time. The intersect is the gelation point, where $G'(\omega) \sim G''(\omega) \sim \omega^n$.

DISCUSSION & CONCLUSIONS: The effects of solvent quality on solution properties, gelation and gel properties are successfully characterised. Concentrated solutions do not show a dependency on solvent quality regarding plateau modulus and therefore entanglement density, as already shown by Graessley [2].

The effects of solvent quality only emerges for completely crystallized gels. It was found that gels derived from poor solvents are stiffer, suggesting a higher crosslink density. Entanglements and crystals contribute to the overall crosslink density, which makes a distinction (based on a dynamic mechanical analysis) difficult.

REFERENCES:

- ¹ R. Schaller; **2015**; *Macromolecules*; Vol 48, 24:8877-8884.
- ² W.W. Graessley; **1980**; *Polymer*; Vol 21, 3:258-.

Nanoconfined water interacting with proteins

Ezgi Bülbül¹, Dirk Hegemann², Manfred Heuberger³

^{1,3} ETH Zürich, Zürich, Switzerland. ^{1,2,3} EMPA St Gallen, St Gallen, Switzerland.

The protein-surface interaction at the solid-liquid interface is of paramount interest in surface sciences such as bio-compatibility, non-fouling and bio-sensing. The suppression of non-specific protein adsorption is sought for the prevention of the initiation of undesired biological reactions. In view of changing surface chemistry to diminish protein adsorption, the water molecules in the vicinity would play an unanticipated role.

Plasma polymerization offers a versatile tool to design subsurface gradient architectures comprising a hydrophilic to hydrophobic gradient for water interaction studies. The control of deposition conditions such as energy input, gas flow rates and deposition rates enables to acquire desired film properties in terms of thickness, surface wettability, density and cross-linking degree¹. Based on the gas phase monomer precursor hexamethyldisiloxane (HMDSO) enabling deposition of highly stable plasma polymer films, the tailored subsurface properties are obtained via precise admixture of different amounts of oxygen to HMDSO in the plasma. Thus, hydrophilic SiOx base layers with varying porosity can be deposited terminated by an nm-thick hydrophobic layer. The response of the gradient matrix to aqueous environments was investigated by neutron reflectometry. Regardless of the hydrophobicity of the terminating layer, penetration of water molecules through gradient is energetically favorable which results in enrichment of water molecules underneath the surface. The impact of this water mediated gradient on protein adsorption was observed via a unique instrument, Transmission Interferometric Adsorption Sensor. It was notably perceived that the protein adsorption is substantially reduced on the hydrated gradient compared to reference surfaces^{2,3}. It is even much more suppressed in the presence of an enhanced hydrated gradient. This remarkable result is attributed to the directional orientation of penetrating water molecules in the designed gradient that yields to the separation of molecules in a distance of 5-6 Å. Hence, the dipole moment of ferro-electric water molecules creates long range interaction forces in the crosslinked sub-region.

To address this hypothesis, the force-distance characteristics of both non-hydrated and hydrated state of films have recently been characterized by Kelvin probe force microscopy. Furthermore, the hydration time effect on protein adsorption kinetics will be examined.

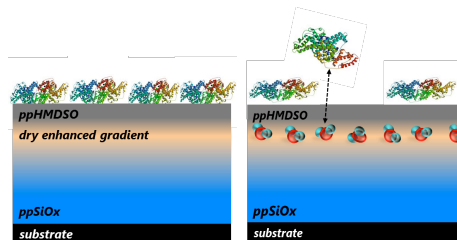


Fig. 1: The effect of hydrated subsurface vertical chemical gradient on protein adsorption

REFERENCES: ¹ Hegemann, D., Design of functional coatings. *Journal of Vacuum Science & Technology A: Vacuum, Surfaces, and Films*, 2005. **23**(1): p. 5-11.

² Hegemann, D., N.E. Blanchard, and M. Heuberger, *Reduced Protein Adsorption on Plasma Polymer Films Comprising Hydrophobic/Hydrophilic Vertical Chemical Gradients*. *Plasma Processes and Polymers*, 2016. **13**(5): p. 494-498.

³ Hegemann, D., N. Hocquard, and M. Heuberger, *Nanoconfined water can orient and cause long-range dipolar interactions with biomolecules*. *Scientific Reports*, 2017. **7**(1): p. 17852.

ACKNOWLEDGEMENTS: This work is financially supported by the Swiss National Science Foundation (project no. 200021_169180).

Novel diblock amphiphilic co-polymer PEO-PEHOx and its self-assembly in aqueous solution

D.Daubian¹

¹ University of Basel, Basel, Switzerland.

INTRODUCTION: Nowadays, a large choice of 2-substituted-2-oxazolines is known, ranging from alkyl-substituted 2-oxazolines to amino, aldehyde, fluorinated and thioethers groups. In particular, Poly(2-methyl-2-oxazoline) as a FDA-approved polymer has been extensively used for the synthesis of a hydrophilic block in amphiphilic block copolymers. But when it comes to hydrophobic blocks, it has rarely been used before due to a lack of a suited poly(2-alkyl-2-oxazolines) with a low T_g .

Kempe et al.¹ overcame this challenge with the synthesis of the first hydrophobic poly(2-oxazoline) with a T_g below 0°C (-6°C), poly(2-(3-ethylheptyl)-2-oxazoline (PEHOx) which has a branched side chains with a total of 9 carbons. This monomer is perfectly suitable as an hydrophobic block in an amphiphilic block copolymers but was never used so far and its self-assembly studied. We hereby report the synthesis of novel diblock copolymers poly(ethylene oxide)-*b*-poly(2-(3-ethylheptyl)-2-oxazoline(PEO-*b*-PEHOx (Figure 1)) using microwave-assisted polymerization.

RESULTS: After a thorough study of the kinetics of the microwave polymerization under various conditions and notably different solvents (acetonitrile, sulfolane, chlorobenzene), we managed to synthesize a series of PEO-PEHOx. (Table 1).

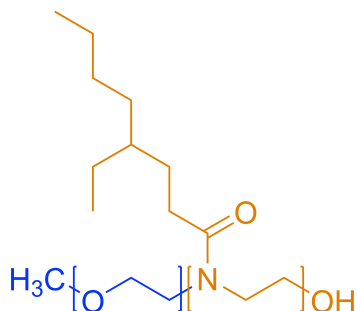


Fig 1: Amphiphilic diblock copolymer PEO-PEHOx

We then studied their self-assembly their self-assembly in aqueous solution using film rehydration.

Polymers	M_n [Da] (¹ H)	\bar{D}_M (GPC)
PEO ₄₅ - <i>b</i> -PEHOx ₄₀	9900	1.27
PEO ₄₅ - <i>b</i> -PEHOx ₄₁	10100	1.29
PEO ₄₅ - <i>b</i> -PEHOx ₄₆	11000	1.32
PEO ₄₅ - <i>b</i> -PEHOx ₅₇	13200	1.36
PEO ₄₅ - <i>b</i> -PEHOx ₆₂	14200	1.35

Table 1 - Library of diblock copolymers PEO-PEHOx. GPC done in chloroform

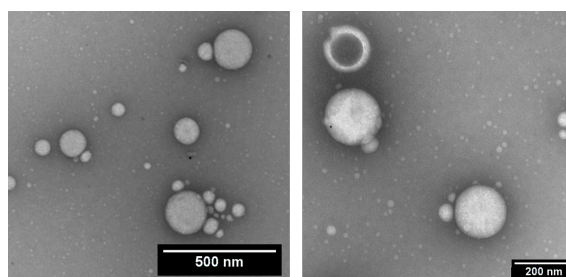


Fig 2: TEM images of PEG₄₅-PEHOx₄₁

DISCUSSION & CONCLUSIONS:

All polymers show a monomodal and narrow molecular weight distribution confirming the controlled character of the polymerization performed. TEM images shows us that all diblocks copolymers self-assembled into spherical objects with radii ranging from 60 to 100 nm (Figure 2). The size of those spherical objects is not uniform. A fraction of micelles are also present. No distinct difference could be observed for different block lengths. Further study by Light scattering and Cryo-TEM would be needed in the future to characterize more indepth those spherical particles.

REFERENCES

1. Kempe, K.; Jacobs, S.; Lambermont-Thijs, H. M. L.; Fijten, M. M. W. M.; Hoogenboom, R.; Schubert, U. S., *Macromolecules* **2010**, *43* (9), 4098-4104.

ACKNOWLEDGEMENTS:

D.Daubian acknowledges the financial support from the Swiss National Science foundation (SNSF) and University of Basel, Switzerland.

How to Determine Material Properties as HSP by Inverse Gas Chromatography

R.Duempelmann¹, E.Brendle²

¹ Inolytix AG, Sisseln, Switzerland. ² Adscientis SARM, Wittelsheim, France.

INTRODUCTION: Many practical chemical products are actually formulations, i.e. sophisticated mixtures like pigments in printing inks or polymers, pharmaceuticals in excipients or plastizers in polymers. The chemistry and the application tests are well known, but the understanding of the interactions is often still very limited. The surface properties of particles and fibres can be determined by a dynamic pulse adsorption, so-called Inverse Gas Chromatography (IGC) ¹. About 20 different gas probes are thereby used to characterize the properties of industrial samples. Recently, the method has been improved to characterize also low-volatile liquids as oligomers, excipients and plastizers in terms of their Hansen Solubility Parameters (HSP) ². The HSP data define the material properties in three dimensions, the disperse, the polar and the hydrogen-bonding properties (δ_D , δ_P , and δ_H), which is used by formulators.

Various "Inverse Chromatography" techniques

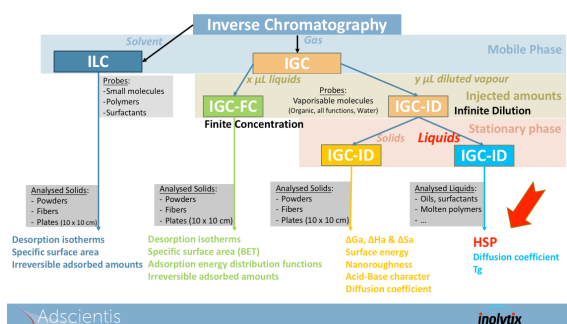


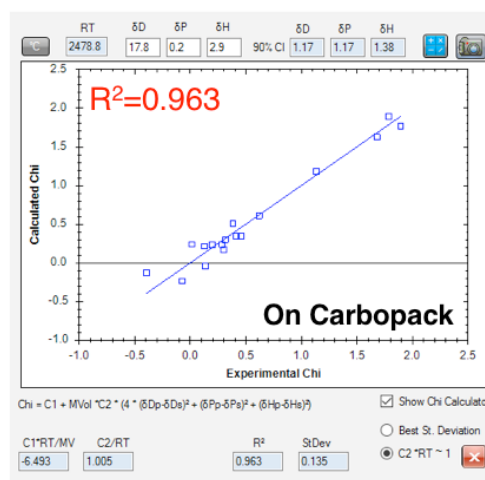
Fig. 1: The systematic of Inverse Gas Chromatography. HSP of liquids is determine under IGC at Infinite Dilution.

METHODS: The liquids of interest are coated with 15-20 wt% on Carpack C80, filled into a 1/4" column, mounted into a GC and conditioned under Helium flow. About 20 different gas probes are pulsed into the He flow at very low concentration (infinite dilution) over the samples to provide the retention times. The gas probes are different in properties covering the HSP sphere ideally.

The resulting net retention volumes are the basis to calculate the Flory-Huggins interaction parameters ($\chi_{1,2}^{\infty}$) and subsequently the unknown HSP of the liquids using the method of Adamska and Voelkel. We use the HSPiP software by S. Abbott which

contains a database and allows the import of the net retention volumes ³.

RESULTS: The HSP determination of commercial samples of excipients and plastizers is mostly very good with correlation coefficients above 0.9 and even small differences are detected, e.g. for modified oligomers. Care must be taken in choosing the inert carrier. The often used Chromosorb P AW-DMDCS shows unfavourable interactions and should be avoided.



HSP: $\delta_D=17.8$; $\delta_P=0.2$; $\delta_H=2.9$

Fig. 2: The regression fit to determine HSP of sesame oil using the HSPiP software.

DISCUSSION & CONCLUSIONS: Around 20 different gas probes are used to determine unknown surface and material properties by a technique called IGC. The HSP data of low-volatile liquids can be determined, but care must be taken in terms of carrier and conditions. This improved technique and data treatment provides formulators very practical guidance in selecting the right additives for the given industrial challenges.

REFERENCES: ¹ E. Brendlé, E. Papirer; **2006**; Surfactant Science Series 137; 48-115

² E. Brendlé, R. Dümpelmann, S. Abbott; **2017**; 50th Anniversary HSP Conference, York, UK.

³ S. Abbott; <https://www.stevenabbott.co.uk/practical-chromatography/hsp.php>

ACKNOWLEDGEMENTS: Steven Abbott's guidance in the HSPiP software and many related questions is greatly acknowledged.

Spontaneous reduction of polydispersity and self-healing colloidal crystals

U. Gasser¹, A. Scotti¹, E.S. Herman², M. Pelaez-Fernandez⁴, L.A. Lyon³, A. Fernandez-Nieves⁴

¹ *Laboratory for Neutron Scattering and Imaging, Paul Scherrer Institut, Villigen, Switzerland.*

² *School of Chemistry and Biochemistry, Georgia Institute of Technology, Atlanta GA, USA.*

³ *Chapman University, Schmid College of Science and Technology, Orange CA, USA.*

⁴ *School of Physics, Georgia Institute of Technology, Atlanta GA, USA.*

INTRODUCTION: Crystallization is often suppressed by the presence of point defects due to larger atoms or impurity particles. Surprisingly, colloidal pNIPAM hydrogels can overcome this limitation: A small number of large microgels can spontaneously deswell to fit in the crystal lattice of smaller but otherwise identical microgels, thus avoiding the occurrence of point defects [1]. We find this unique reduction of polydispersity and particle deswelling to be due to an osmotic pressure difference between the inside and the outside of the microgels [2].

METHODS: We have directly observed the deswelling of pNIPAM microgels in concentrated samples at fixed temperature, $T \sim 18^\circ\text{C}$, using small-angle neutron scattering (SANS) with contrast matching. Bidisperse suspensions with a small number of large particles added to a suspension of small particles have been studied. The osmotic pressure in the same samples was determined with a membrane osmometer. Small-angle X-ray scattering (SAXS) was used to determine the phase behavior of bidisperse suspensions with number fractions of large particles between 1% and 70% and also of polydisperse suspensions with polydispersities in the range from 9% up to 20%.

RESULTS: Our SANS measurements show the selective deswelling of the large pNIPAM microgels in bidisperse suspensions with effective volume fractions above a critical value to depend on the fraction of large particles present in the suspension. The osmotic pressure, Π , is found to be compatible with ideal gas behavior at low effective volume fractions $\zeta \leq 0.8$. At higher ζ , the increase of Π becomes significantly steeper.

Our SAXS results on bidisperse suspensions reveal a strong dependence of the freezing, ζ_f , and melting, ζ_m , points on the fraction of large particles in the suspension, n_b . Both shift to higher ζ with increasing n_b , and the coexistence regime gets narrower. Crystals are not observed for $n_b \geq 0.3$. Polydisperse suspensions show a similar behavior with crystallization being suppressed for polydispersities $> 19\%$, significantly higher than the 12% limit in hard spheres.

DISCUSSION & CONCLUSIONS: Although pNIPAM is an uncharged polymer, pNIPAM microgels carry charged groups on their surface, which are due to the starter for the polymerization reaction. Most of the counterions of the charged

groups are trapped close to the microgel surface, but a fraction of them escapes and sets the osmotic pressure of the suspension. The counterion clouds of neighboring particles progressively overlap with increasing ζ , leading to an increase of free counterions and the osmotic pressure. This increase of osmotic pressure outside the particles is not compensated by a pressure increase inside the particles and, therefore, the particles deswell when the pressure difference gets larger than their bulk modulus (see Fig. 1). Large particles are softer than small ones synthesized following the same protocol and, therefore, the larger particles deswell first.

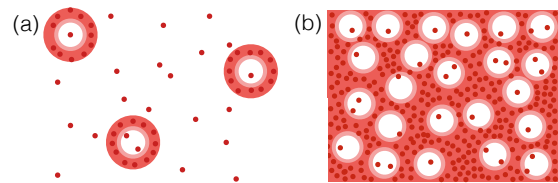


Fig. 1: (a) Sketch of a dilute suspension with most counterions trapped close to the particle surface (red rings) and a small fraction of free counterions (red dots). (b) Concentrated suspension with overlapping counterion clouds.

We find the freezing point of bidisperse pNIPAM suspensions to be determined by particle deswelling [3]: A reduction of polydispersity due to the deswelling of the large particles in the bidisperse suspensions is required for crystallization. Compared to monodisperse suspensions, this causes the freezing point to shift to higher concentrations.

CONCLUSIONS: Compared to hard colloidal particles, the spontaneous particle deswelling of soft pNIPAM particles [2] fundamentally changes the role of polydispersity in pNIPAM suspensions and possibly other soft polymer particles. New models for the phase behavior of soft polymer particles including spontaneous deswelling above a critical concentration are needed.

REFERENCES:

- (1) A. St. Iyer and L.A. Lyon, *Angew. Chem. Int. Ed.* 48, 4562-4566 (2009).
- (2) A. Scotti, U. Gasser, E.S. Herman, M. Pelaez-Fernandez, J. Han, A. Menzel, L.A. Lyon, A. Fernandez-Nieves, *PNAS* 113, 5576-5581 (2016).
- (3) A. Scotti, U. Gasser, E.S. Herman, J. Han, A. Menzel, L.A. Lyon, A. Fernandez-Nieves, *Pys. Rev. E* 96, 032609 (2017).

An alternative laboratory method for solid-state biaxial stretching of polymers: from single to multilayer films

Gagik Ghazaryan, Jan Vermant, Theo A. Tervoort

Department of Materials, ETH Zurich, Switzerland

Biaxial stretching of polymers is a common processing technology for the production of films in numerous applications, including food packaging and labels. There are two primary industrial processes for production of biaxially oriented films, the tenter frame method and the double-bubble method. While the former method is mainly used to produce mono-layer films, the latter one is also used for biaxial stretching of multi-layer films and has recently been extended to the so-called “triple-bubble” method, where the last bubble allows for setting of the film after biaxial deformation [1]. The aforementioned industrial methods require large and expensive equipment as well as large amounts of materials. Therefore, several types of techniques have been utilized to investigate the biaxial stretching of films on a laboratory scale. However, these small-scale methods do not allow for continuous drawing and often result in non-homogeneously oriented samples.

In this study we present a lab-scale method to produce biaxially oriented films which emulates, to some extent, the triple-bubble process. The method involves biaxial solid-state deformation of a polymer precursor tube over a heated V-shaped metal mandrel. Both the feeding speed of the tube as well as the pulling rate of the film are perfectly controlled, which ensures production of biaxially oriented films with controlled in-plane orientation in the machine and transverse directions. The process of biaxial deformation is modelled theoretically, assuming that the stress during plastic deformation of the polymer at elevated temperatures mimics the stress in a cross-linked rubber. The experimental data accurately coincide with our theoretical model.

Finally, we applied our method to two case studies. Firstly, biaxially oriented films were produced from single layer poly(L-lactic acid) (PLLA) tubes. As expected, the solid-state biaxial stretching enhanced the mechanical properties of PLLA. In contrast to non-oriented PLLA films, the biaxially oriented films showed no sign of embrittlement and the improved mechanical properties were conserved during the physical aging for a period of a month [2]. Secondly, triple-layer tubes, comprising polyethylene terephthalate (PET), a tie layer and isotactic polypropylene (*i*-PP), were biaxially stretched to produce balanced films. First results of the adhesive properties of these films will be reported, showing that the adhesion force of these multi-layer films, as measured by T-peel testing, strongly depends upon whether or not the tie layer is in the molten state during the biaxial stretching.

References

- [1] DeMeuse, M. T. *Biaxial stretching of film*, Woodhead Publishing: Cambridge, UK, 2011.
- [2] Ghazaryan, G.; Schaller, R.; Feldman, K.; Tervoort, A. T., *J. Polym. Sci. B: Polym. Phys.* **2016**, *54*, 2233-2244.

Cellular integration of preorganized artificial organelle networks

J. Liu¹, I. Craciun¹, A. Belluati¹, M. Chami¹, C. Palivan¹

¹ University of Basel, Basel, Switzerland

INTRODUCTION: Various pathologic conditions require complex solutions for which nanoscience-based systems are essential. The development of artificial organelles represents an elegant approach to provide enzymatic reactions in protected spaces to produce the required compounds inside cells. In particular artificial organelles organized into sub-micrometer sized clusters mediated by DNA, enable the synchronization and the incorporation of different functional blocks to amplify and expand their functions, compensating the shortage of nano-sized compartments with limited interior space. Cellular integration of artificial organelle networks would allow the mimics of metabolic processes in cells as well as the fabrication of complex and intelligent nanosystems for therapeutic and diagnostic applications.

METHODS: poly(dimethylsiloxane)-*block*-poly(2-methyloxazoline) (PDMS₆₂-PMOXA₁₃) was combined with 20 mol% of PDMS₇₁-PMOXA₂₅-OEG₃-N₃ for the self-assembly of polymersomes by film rehydration method. The azide-functionalized diblock copolymers with longer PMOXA block enable the protrusion of azide groups out of polymersome's surface for the linkage of dibenzocyclooctyne (DBCO)-functionalized 11-bp and 22-bp ssDNA (DBCO-ssDNA) by strain-promoted azide-alkyne cycloaddition (SPAAC). The morphology of polymersomes and ssDNA-functionalized polymersomes was characterized by transmission electron microscopy (TEM) and dynamic light scattering (DLS) and the number of ssDNA per polymersome was determined by fluorescence correlation spectroscopy (FCS). ATTO 488 and DY-633 dyes were encapsulated in complementary polymersomes, respectively, for the visualization by confocal laser scanning microscopy (CLSM). Afterwards, polymersome clusters was formed by incubating complementary ssDNA-polymersomes at 37 °C and they were characterized by TEM and DLS. The stability of polymersome clusters linked by 11-bp and 22-bp ssDNA in the presence of DNase I was investigated by the combination of cryo-TEM, DLS and TEM. In the end, we examined their interactions with respect to two epithelial (HeLa and HEK293T) and a glioblastoma (U87-MG) cell line, to determine if the polymersome clusters have any inherent selectivity towards a specific cell line.

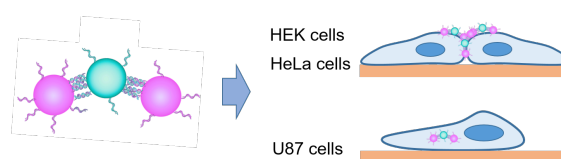


Figure 1: Selective interactions of polymersome clusters with different cell lines.

RESULTS: Polymersome clusters with different sizes have been constructed. The height of DNA layer between linked polymersomes determines their stability against nuclease digestion. The preorganized clusters interact with cells mediated by scavenger receptor and exhibit different scenarios with distinct types of cells: they showed high cell uptake when incubated with U87 cells, while were strongly attached on the surface of HEK and HeLa cells.

DISCUSSION & CONCLUSIONS:

Artificial organelle networks with different size and architecture have been integrated into cells with high efficiency and negligible toxicity. Importantly, such preorganized artificial organelle networks are capable to assist the colocalization of polymersome building blocks *in vitro*, paving the way for the implantation of multiple nano-objects that are required to function in tandem as well as the repair and the modification of signaling pathway by synthetic materials in cells.

Surface-grafted Polymer Brushes as Artificial Environment for Functional Enzymes

J. Razumovitch¹, V.J. Cadarso², C. Padeste¹

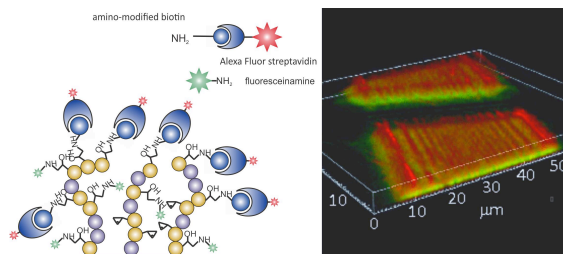
¹ *Paul Scherrer Institut, Villigen, Switzerland*

² *Monash University, Clayton, Australia*

INTRODUCTION: Modern medicine and biotechnology demand the quick development of smart biosurfaces with the ability to firmly anchor biomolecules without impairing their solution properties. Surface-grafted polymer brushes are considered ideal candidates to provide an environment suitable for incorporation of functional enzymes. By selection of monomers or their post-polymerization functionalization the physical and chemical properties of brushes can be tuned for specific applications. For the implementation for biosensor applications some additional factors must be taken in to account: The proteins should have constant concentration, which can be provided by covalent coupling proteins to brushes, and a certain conformational freedom to be functional within the brushes.

The aim of this project is to develop a technology for grafting of biofunctional polymer brushes and for the investigation of protein activity in the artificial surface-bound state.

METHODS: Polymer brushes were synthesized using a “grafting-from” strategy based on extreme ultraviolet radiation used to create patterns of radical initiators at the surface of poly(ethylene-alt-tetrafluoroethylene) foils by free radical polymerization. Using the IR-spectroscopy and Scanning Probe Microscopy methods we investigated the influence of the ratio of N-vinylpyrrolidone (VP) and glycidyl methacrylate (GMA) monomers on the physical and chemical properties of polymer brushes, such as thickness and relative amount of reactive epoxy groups. The biotin-streptavidin model was used to prove the concept of biofunctionalization of poly(GMA-co-VP) brushes. In order to test the enzymatic activity of proteins coupled to the brushes a microfluidic setup based on spectrophotometric measurements was developed. As a model enzyme horseradish peroxidase (HRP) was used, which catalyzes the transformation of a colorless substrate into a colored product, and its enzymatic activity can therefore be easily monitored with colorimetry.



Laser Scanning Microscopy images of functionalized poly(GMA-co-VP) brush structures.

RESULTS: The thickness and density of grafted polymer brushes depend on surface radical density (exposure dose) and volume ratio of monomers. Fluorescent patterns of dyes linked to polymer brushes repeat the surface radical patterns obtained after EUV exposure. In dose-dependent manner proteins bind with higher yield to surface-located epoxy groups or epoxy groups on long (meaning more flexible) polymer chains (Figure 1). Poly(GMA-co-VP) brushes can provide a convenient artificial environment for HRP, which keeps a steady enzymatic activity within the brushes during several reaction cycles.

DISCUSSION & CONCLUSIONS: The results indicate a great potential of polymer brush-protein systems for the development of stable and robust biosensors.

Extreme ultraviolet (EUV) lithography is a perfect tool to create radical patterns at polymer surfaces for “grafting from” of polymer brushes and to allow subsequent characterization.

Copolymerization of VP and GMA in various volume ratios allows to tune the brush hydrophilicity and epoxy group concentration in order to obtain an optimal environment for incorporation of functional enzymes.

Figure 1: Biofunctional polymer brushes: schematic view and 3D reconstruction of Confocal

Immobilizing vesicles through catalyst free click reaction

S. Rigo, G. Gunkel-Grabole, C. G. Palivan*

Department Physical Chemistry, University of Basel, Mattenstrasse 24a, CH-4058 Basel, Switzerland.

INTRODUCTION: Immobilizing self-assembled structures on a solid support gained lot of interest in the last years as they have various potential applications, medical or as sensors. Covalent and non-covalent immobilization methods were established. Copper(I) catalyzed azide alkyne cycloaddition (CuAAC) is a well-known, chemo-selective click reaction, which is applied in a wide range of fields in chemistry and biology. CuSO_4 with the reducing agent ascorbate is often used to in situ produce catalytically active Cu(I) and thereby catalyzing this click reaction. One limitation, however, is the cytotoxicity of Cu(I). Copper and catalyst free click reactions were developed. The strain promoted Azide-Alkyne click (SPAAC) reaction is based on the high reactivity of alkynes in an 8-membered ring.[1] Here we introduced this biorthogonal, catalyst free click reaction to immobilize polymersomes on a solid support. This is promising to engineer smart surfaces for medical [2] or sensing purposes due to low toxicity, high selectivity and rapid immobilization kinetics.

METHODS: Surfaces are functionalized by silane chemistry with (3-Aminopropyl)triethoxysilane (APTES) and further by amide formation of amine with carboxylic acid (Figure 1). The surfaces are characterized by contact angle (CA) measurements and scanning microscopy (LSM).

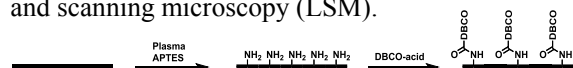


Figure 1: Schematic representation of the surface functionalization.

Poly(2-methylloxazoline)-*block*-poly(dimethylsiloxane)-*block*-poly(2-methylloxazoline) (PMOXA-*b*-PDMS-*b*-PMOXA) based polymersomes with different ratios of azide terminated polymers were prepared by thin film rehydration and characterized by transmission electron microscopy (TEM), dynamic light scattering (DLS) and fluorescence correlation spectroscopy (FCS). Polymersomes are immobilized overnight and studied by LSM, atomic force microscopy (AFM) and scanning electron microscopy (SEM).

RESULTS: Successful functionalisation of the surface with DBCO groups has been shown by an

increase of CA and immobilization of an azide dye through SPAAC reaction and visualized by LSM. Polymersomes with azide groups were stable and their presence did neither affect the self-assembly process nor the architecture, as characterized by DLS and TEM. Surfaces with immobilized polymersomes were achieved after overnight reaction of the polymersomes with the surface. Changing the ratio between 0.1% and 10% N_3 terminated polymers in the polymersomes did not affect the immobilization of them.

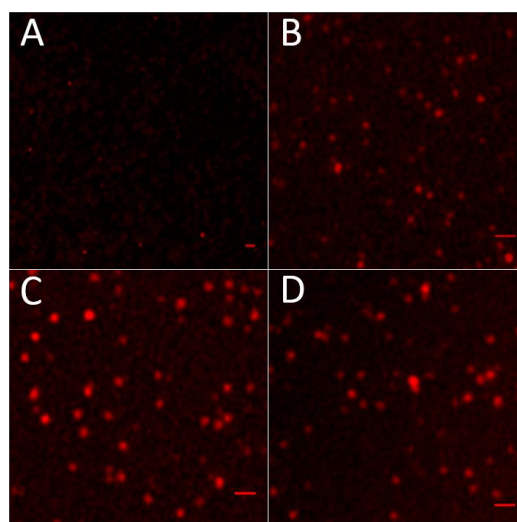


Figure 2: LSM images of immobilized bodipy stained vesicles with different ratio of N_3 terminated polymers A) 0% B) 0.1% C) 1% D) 10% on DBCO functionalized surfaces. Scale bar: 1 μm .

DISCUSSION & CONCLUSIONS: The immobilization of polymersomes has been achieved by reacting the DBCO functionalized surface with the azid functionalized polymersomes overnight. Next, the immobilization of catalytically active nanocompartments to produce smart surfaces will be studied.

REFERENCES: ¹ N. J. Agard; **2004**; *JACS*; 126:15046-15047. ² K. Langowska; **2013**; *Chem. Commun.*; 49:128-130.

ACKNOWLEDGEMENTS: Financial support was provided by Swiss National Science Foundation (SNSF), which is gratefully acknowledged. We thank Samuel Lörcher for polymer synthesis.

Developing Self-Assembled Peptide Nanoparticles for Safe and Efficient Gene Delivery

Shabnam Tarvirdipour^{1,2*}, Cora-Ann Schoenenberger¹, Yaakov Benenson², Cornelia G. Palivan¹

¹ Department of Chemistry, University of Basel, Basel, Switzerland

² Department of Biosystems Science and Engineering, ETH Zürich, Basel, Switzerland

INTRODUCTION: Gene therapy involves delivering genetic material to the nucleus of recipient cells by viral or non-viral delivery systems [1,2]. Today, non-viral strategies with DNA encapsulated/entrapped inside nanometer-sized systems (e.g. micelles, nanoparticles, vesicles) gain increasing attention because they offer several advantages including the safety profile, localized gene expression and cost-effectiveness [3]. We are exploring peptide-based nanostructures that represent a type of biodegradable non-viral vector with extensive design options and generally low cytotoxicity. Specifically, we synthesized and purified the amphiphilic H3gT peptide which consists of 10 amino acids and examined its self-assembly in the presence of a single-stranded oligonucleotide.

METHODS: A Liberty Blue-Microwave peptide synthesizer (CEM, Kamp-Lintfort, Germany) was used to synthesize H3gT. The synthesis was performed on a rink amide resin using standard fluorenylmethoxycarbonyl (Fmoc) solid phase peptide synthesizer chemistry and DIC/OXYMA coupling methods. Analytical high performance liquid chromatography (HPLC) and liquid chromatography mass spectrometry (LC-MS) was done before and after peptide purification. DNA loaded peptide supra-molecular assemblies were prepared by adding 4 μ L of 100 μ M 22mer ssDNA solution to 100 μ L peptide solution (1 mg/mL) and the further diluting the mixture with 500 μ L 35% ethanol. Dynamic light scattering (DLS), zeta potential measurements, fluorescence correlation spectroscopy (FCS), transmission electron microscope (TEM) were used to characterize the resulting self-assembled nanostructures.

RESULTS: DNA-loaded peptide assemblies have a size below 200 nm (Fig. 1A) with a neutral surface charge, which indicates that the 22mer is entrapped inside the assembly. TEM revealed spherical nanoparticles (Fig. 1B). Moreover, FCS data showed a 67% entrapment efficiency (Fig. 1C). In order to evaluate whether the DNA concentration affects the H3gT self-assembly, three different 22mer concentrations (0.8; 1.6; 3.2 μ g/ml) were tested (Fig. 2 A, B and C, Table 1). Distinct nanoparticles were found at 0.8 and 1.6 μ g/ml, whereas higher DNA concentrations induced aggregation.

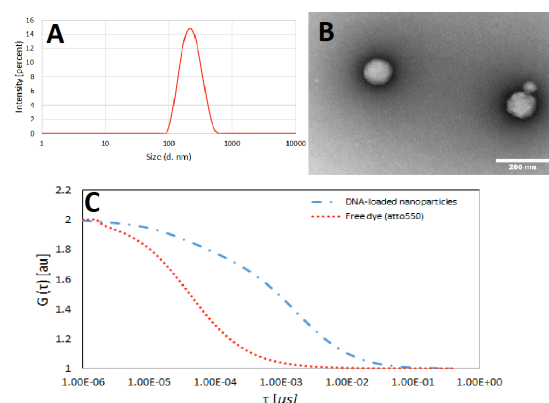


Fig. 1 (A), DLS and (B) TEM micrograph of DNA-loaded H3gT peptide nanoparticles; (C) FCS autocorrelation curves for free ATTO550 (red), and ATTO550-DNA-loaded peptide assemblies (blue). Scale bar = 200nm.

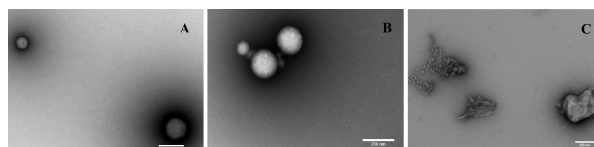


Fig. 2 TEM micrographs of H3gT peptides after self-assembly in the presence of ssDNA: (A) 0.8 μ g/ml 22mer, 1.6 μ g/ml 22mer, (C) 3.2 μ g/ml 22mer. Scale bar = 200nm.

Table 1. Size of peptide nanostructures assembled in the presence of different concentrations of ssDNA.

DNA Conc. (μ g/ml)	0.8	1.6	3.2
Hydrodynamic diameter (nm)	120 \pm 40	200 \pm 11	420 \pm 30
Aggregation	-	-	✓

DISCUSSION & CONCLUSIONS: We successfully entrapped 22-mer DNA strands inside the H3gT peptide nanoparticles via electrostatic interaction with the histidine domain. These results serve as input data to further improve our non-viral delivery system by modifying H3gT peptide to allow for entrapment of higher molecular mass single- and double stranded DNA.

REFERENCES: ¹ M. Ramamoorth, A. Narvekar; **2015**; JCDR; 9(1):GE01.

² S.J. Sigg, *et al.*, *Biomacromolecules*, **2016**; 17(3): 935-945.

³ M. Foldvari *et al.*, **2016**; *Journal of Controlled Release*, 240: 165-190.

Participants

Mr.	Stefan	Aeby	University of Fribourg	Switzerland	stefan.aeby@unifr.ch
Mrs.	Claire	Alais	ETH Zürich	Switzerland	alaisc@student.ethz.ch
Dr.	Alexandra	Alicke	ETH Zürich	Switzerland	alexandra.alicke@mat.ethz.ch
Dr.	Laura	Alvarez Frances	ETH Zurich	Switzerland	laura.alvarez-frances@mat.ethz.ch
Mr.	Mario	Arcari	ETH Zürich	Switzerland	mario.arcari@hest.ethz.ch
Mr.	Robert	Axelrod	ETH Zürich	Switzerland	raxelrod@student.ethz.ch
Mr.	Johannes	Bergmann	University of Fribourg	Switzerland	johannes.bergmann@unifr.ch
Mrs.	Victoria	Blair	ETH Zürich	Switzerland	victoria.blair@mat.ethz.ch
Mr.	Daniel	Blatman	Paul Scherrer Institut	Switzerland	Daniel.Blatman@psi.ch
Mr.	Peter	Bohnacker	ETH Zürich	Switzerland	peterbo@student.ethz.ch
Mr.	Enzo	Bomal	EPFL	Switzerland	enzo.bomal@epfl.ch
Mr.	André	Brem	ETH Zürich	Switzerland	abrem@mat.ethz.ch
Mrs.	Ezgi	Bülbül	EMPA St Gallen	Switzerland	ezgi.buelbuel@empa.ch
Prof.	Adam	Burbidge	Nestec SA	Switzerland	adam.burbidge@rdls.nestle.com
Mr.	Gabriele	Colombo	ETH Zürich	Switzerland	gabriele.colombo@mat.ethz.ch
Mr.	Davy	Daubian	University of Basel	Switzerland	davy.daubian@unibas.ch
Mr.	Michael	Diener	ETH Zürich	Switzerland	michael.diener@hest.ethz.ch
Mr.	Kilian	Dietrich	ETH Zürich	Switzerland	kilian.dietrich@mat.ethz.ch
Dr.	Ralf	Duempelmann	Inolytix AG	Switzerland	ralf.duempelmann@inolytix.com
Dr.	Kirill	Feldman	ETH Zurich	Switzerland	kfeldman@mat.ethz.ch
Dr.	Maria	Feofilova	ETH Zurich	Switzerland	maria.feofilova@mat.ethz.ch
Prof.	Alberto	Fernandez-Nieves	Georgia Institute of Technology	USA	alberto.fernandez@physics.gatech.edu
Dr.	Miguel Angel	Fernandez-Rodriguez	ETH Zurich	Switzerland	ma.fernandez@mat.ethz.ch
Mr.	Jonas	Freitag	ETH Zurich	Switzerland	jfreitag@student.ethz.ch
Dr.	Urs	Gasser	Paul Scherrer Institut	Switzerland	urs.gasser@psi.ch

Dr.	Thomas	Geue	Paul Scherrer Institut	Switzerland	thomas.geue@psi.ch
Mr.	Reza	Ghanbari	ETH Zurich	Switzerland	reza.ghanbari@hest.ethz.ch
Mr.	Gagik	Ghazaryan	ETH Zurich	Switzerland	gagik.ghazaryan@mat.ethz.ch
Dr.	Yogesh	Harshe	Nestle Research Center	Switzerland	yogesh.harshe@rdls.nestle.com
Mr.	Chiao-Peng	Hsu	ETH Zürich	Switzerland	chiao-peng.hsu@mat.ethz.ch
Prof.	Lucio	Isa	ETH Zurich	Switzerland	lucio.isa@mat.ethz.ch
Dr.	Joachim	Kohlbrecher	Paul Scherrer Institut	Switzerland	joachim.kohlbrecher@psi.ch
Mrs.	Karolina	Korzeb	Adolphe Merkle Institute, University of Fribourg	Switzerland	karolinakorzeb@gmail.com
Mr.	Nico	Kummer	ETH Zürich	Switzerland	kummern@student.ethz.ch
Mrs.	Myrto	Kyropoulou	University of Basel	Switzerland	myrto.kyropoulou@unibas.ch
Dr.	Juan	Liu	University of Basel	Switzerland	juan.liu@unibas.ch
Mr.	Byron	Llerena	ETH Zurich	Switzerland	byronl@ethz.ch
Dr.	Viviane	Lutz-Bueno	Paul Scherrer Institut	Switzerland	viviane.lutz-bueno@psi.ch
Mrs.	Stefanie	Neuhaus	University	Switzerland	stefanie.neuhaus@unifr.ch
Dr.	François	Peaudecerf	ETH Zürich	Switzerland	peaudecerf@ifu.baug.ethz.ch
Mr.	Roberto	Pioli	ETH Zurich	Switzerland	pioli@ifu.baug.ethz.ch
Dr.	Julia	Razumovitch	Paul Scherrer Institut	Switzerland	julia.razumovitch@psi.ch
Dr.	Damian	Renggli	ETH Zurich	Switzerland	damian.renggli@mat.ethz.ch
Mrs.	Serena	Rigo	University of Basel	Switzerland	serena.rigo@unibas.ch
Mr.	Ilya	Savchenko	ETH Zurich	Switzerland	ilya.savchenko@hest.ethz.ch
Mrs.	Laura	Scheidegger	ETH Zürich	Switzerland	laura.scheidegger@mat.ethz.ch
Dr.	Cora-Ann	Schoenenberger	University of Basel	Switzerland	Cora-Ann.Schoenenberger@unibas.ch
Mr.	Bram	Schroyen	ETH Zurich	Switzerland	bram.schroyen@mat.ethz.ch
Dr.	Nesrin	Senbil	University of Fribourg	Switzerland	nesrin.senbil@unifr.ch
Mrs.	Alba	Sicher	Empa	Switzerland	alba.sicher@empa.ch
Mr.	Hendrik	Spanke	ETH Zürich	Switzerland	hendrik.spanke@mat.ethz.ch

Mr.	Sandro	Stucki	ETH Zurich	Switzerland	stuckis@student.ethz.ch
Mrs.	Shabnam	Tarvirdipour	University of Basel	Switzerland	shabnam.tarvirdipour@unibas.ch
Prof.	Theo	Tervoort	ETH Zurich	Switzerland	tervoort@ethz.ch
Dr.	Andrea	Testa	ETH Zurich	Switzerland	andrea.testa@mat.ethz.ch
Mrs.	Alexandra	Thoma	ETH Zurich	Switzerland	althoma@student.ethz.ch
Dr.	Gregor	Trefalt	University of Geneva	Switzerland	gregor.trefalt@unige.ch
Mr.	Mattia	Usuelli	ETH Zürich	Switzerland	mattia.usuelli@hest.ethz.ch
Dr.	Leonie	van 't Hag	ETH Zurich	Switzerland	leonie.vant@hest.ethz.ch
Mr.	Siddarth	Vasudevan	ETH Zurich	Switzerland	siddarth.vasudevan@mat.ethz.ch
Dr.	Qin	Xu	ETH Zurich	Switzerland	qin.xu@mat.ethz.ch
Dr.	Pavel	Yazhgur	University of Fribourg	Switzerland	pavel.yazhgur@unifr.ch
Mr.	Michele	Zanini	ETH Zurich	Switzerland	michele.zanini@mat.ethz.ch
Dr.	Tao	Zhou	ETH Zurich	Switzerland	tao.zhou@hest.ethz.ch